UNIVERSIDADE FEDERAL DE MINAS GERAIS
Instituto de Ciencias Exatas
Programa de pós-graduação em Física

Túlio Henrique Lopes Gomes de Castro

Optical properties of transition metal dichalcogenides heterostructures

MoS_2/WS_2 Heterojunctions

Belo Horizonte
January, 2023

Túlio Henrique Lopes Gomes de Castro

Optical properties of transition metal dichalcogenides heterostructures

MoS_2/WS_2 Heterojunctions

This version of the thesis includes the corrections and modifications suggested by the Examining Committee during the defense of the original version of the work, which took place on January 17, 2023.

A copy of the original version is available at the Physics department of the federal University of Minas Gerais.

Examining Committee:

Paulo Sergio Soares Guimarães (Advisor)
Prof. Luiz Gustavo de Oliveira Lopes Cançado
Prof. Matheus Josué de Souza Matos

Belo Horizonte
January, 2023

Dados Internacionais de Catalogação na Publicação (CIP)

C355o Castro, Túlio Henrique Lopes Gomes de.
Optical properties of transition metal dichalcogenides heterostructures MoS_2/WS_2 heterojunctions / Túlio Henrique Lopes Gomes de Castro. – 2023.
60f. : il.

Orientador: Paulo Sérgio Soares Guimarães.
Dissertação (mestrado) – Universidade Federal de Minas Gerais, Departamento de Física.
Bibliografia: f. 52-57.

1. Heteroestruturas semicondutoras. 2. Transferência de carga. 3. Metais de transição. I. Título. II. Guimarães, Paulo Sérgio Soares. III. Universidade Federal de Minas Gerais, Departamento de Física.

CDU – 535 (043)

Ficha catalográfica elaborada por Romário Martins Ribeiro – CRB6 3595
Biblioteca Professor Manoel Lopes de Siqueira – Departamento de Física - UFMG

UNIVERSIDADE FEDERAL DE MINAS GERAIS
INSTITUTO DE CIÊNCIAS EXATAS
PROGRAMA DE PÓS-GRADUAÇÃO EM FÍSICA

FOLHA DE APROVAÇÃO

A presente dissertação, intitulada **"Optical properties of transition metal dichalcogenides heterostructures: MoS_2/WS_2 Heterojunctions"**, de autoria de **TÚLIO HENRIQUE LOPES GOMES DE CASTRO**, submetida à Comissão Examinadora, abaixo-assinada, foi aprovada para obtenção do grau de **MESTRE EM FÍSICA** em vinte de janeiro de 2023.

Belo Horizonte, 20 de janeiro de 2023.

Prof. Paulo Sérgio Soares Guimarães
Orientador do aluno
Departamento de Física/UFMG

Prof. Luiz Gustavo de Oliveira Lopes Cançado
Departamento de Física/UFMG

Prof. Matheus Josué de Souza Matos
Departamento de Física/UFOP

Documento assinado eletronicamente por **Matheus Josué de Souza Matos**, **Usuário Externo**, em 23/01/2023, às 09:57, conforme horário oficial de Brasília, com fundamento no art. 5º do Decreto nº 10.543, de 13 de novembro de 2020.

Documento assinado eletronicamente por **Luiz Gustavo de Oliveira Lopes Cancado**, **Professor do Magistério Superior**, em 23/01/2023, às 12:52, conforme horário oficial de Brasília, com fundamento no art. 5º do Decreto nº 10.543, de 13 de novembro de 2020.

Documento assinado eletronicamente por **Paulo Sergio Soares Guimaraes**, **Professor do Magistério Superior**, em 23/01/2023, às 13:51, conforme horário oficial de Brasília, com fundamento no art. 5º do Decreto nº 10.543, de 13 de novembro de 2020.

A autenticidade deste documento pode ser conferida no site https://sei.ufmg.br/sei/controlador_externo.php?acao=documento_conferir&id_orgao_acesso_externo=0, informando o código verificador **2033226** e o código CRC **63A79327**.

Referência: Processo nº 23072.203308/2023-61 SEI nº 2033226

Para Débora e Maíra, sem as
quais eu não teria chegado aqui.

Agradecimentos

Tenho facilidade em ter dificuldades!
— Maurílio dos Anjos

Esse trabalho é fruto de 3 anos de muito trabalho colaborativo. Aqui temos o resultado de todos os erros que cometi e que só pude superar com o apoio e ajuda de várias pessoas. Em primeiro lugar devo muitos agradecimentos ao meu orientador Paulo Sérgio que, ao contrário do que ele diz, fez muito mais do que era sua obrigação como orientador e me guiou pelos caminhos tortuosos que eu decidi percorrer. Obrigado Paulo, pelos ensinamentos, pelo suporte intelectual e financeiro. Você sempre correu atrás de soluções pra todos os obstáculos que enfrentei e me senti muito mais seguro e confiante tendo você como orientador.

Aos companheiros de laboratório que hoje eu considero como meus amigos. Obrigado Juliana por todas as suas maravilhosas sugestões, sempre questionando e me ensinando a questionar tudo, confabulando comigo e debatendo ideias, mas principalmente gostaria de te agradecer pelas conversas. A vida é mais do que ciência e você me ajuda muito a não perder perspectiva da nossa realidade. Obrigado Rafael, você foi um veterano perfeito, me recebeu muito bem no laboratório, compartilhou o conhecimento e sempre se dispôs a me ajudar e ensinar. Algumas das minhas principais qualidades como físico experimental vieram de você e por isso sempre lhe sou grato. E por fim, Obrigado Henrique por toda a companhia e conversas, você é uma das poucas pessoas em todo o meu percurso universitário com quem eu compartilho origens e, por tanto, há coisas que só você entende e se dispôs a ouvir meus desabafos. Obrigado também por todas as noites de cinema no laboratório e os debates culturais.

Gostaria de agradecer a minha mãe e amigos que me ajudaram a não entrar em desespero nos momentos mais difíceis. Obrigado Mãe por sempre me apoiar e aceitar as minhas escolhas de vida mesmo nem sempre concordando. Maíra, obrigado por estar sempre ao meu lado. Os chás as conversas e os momentos com você foram essências para que eu passasse por mais essa etapa. Obrigado a André e Hebert, as amizades com quem eu

sempre posso conversar fora do meio acadêmico.

Por fim, agradeço às agências de fomento, Capes, CNPq e Fapemig, cujo apoio financeiro permitiu que este trabalho pudesse ser concluído. Muito obrigada.

Resumo

Túlio Henrique Lopes Gomes de Castro. **Comportamento Óptico de heteroestruturas de dicalcogenetos de metais de transição: *MoS_2/WS_2 Heterojunctions***. Dissertação (Mestrado). Departamento de Física, Universidade Federal de Minas Gerais, Minas Gerais, 2023.

O estudo de heteroestruturas semicondutoras bidimensionais é de grande interesse para aplicações como a implementação de células solares e vários dispositivos em nanoescala, como transistores de efeito de campo de túnel. Nosso foco neste trabalho foi entender como a interação entre diferentes monocamadas de dicalcogenetos de metais de transição (TMDs) em heteroestruturas verticais afeta suas propriedades ópticas. Estamos particularmente interessados em como ocorrem os processos de troca de energia e carga, e na formação de éxcitons entre-camadas. Estudamos a dependência da fotoluminescência com a temperatura e a potência de excitação além da espectroscopia Raman e microscopia de força atômica, utilizadas para a caracterização das amostras. Encontramos evidências de um mecanismo de transferência de energia entre éxcitons de diferentes camadas quando estão em contato direto, enquanto em camadas separadas por uma fina camada de h-BN vemos uma transferência de carga via tunelamento através dessa camada de h-BN.

Palavras-chave: TMDs. Heteroestruturas. Monocamadas. MoS_2. WS_2. FRET. transferência de carga.

Abstract

Túlio Henrique Lopes Gomes de Castro. **Optical properties of transition metal dichalcogenides heterostructures: *Heterojunções de MoS2/WS2***. Thesis (Master's). Physics Department at Federal University of Minas Gerais, Minas Gerais, 2023.

The study of two-dimensional semiconductor heterostructures is of great interest for applications such as the implementation of solar cells and various nanoscale devices such as tunnel field effect transistors. Our focus in this work was to understand how the interaction between different monolayers of transition metal dichalcogenides in vertical heterostructures affects their optical properties. We are particularly interested in how energy and charge exchange processes take place, and in the formation of interlayer excitons. We studied the photoluminescence dependence on temperature and excitation power in addition to Raman spectroscopy and atomic force microscopy, used for the characterization of the samples. We find evidence of an energy transfer mechanism between excitons of different layers when they are in direct contact, while in layers separated by a thin h-BN layer we see a charge transfer via tunneling through this h-BN layer.

Keywords: TMDs. Heterostructures. Monolayers. MoS_2. WS_2. FRET. Charge Transfer.

List of Tables

2.1 Young's module. 27
2.2 Band-Gap and Binding energies 28

4.1 Slope of the linear relation of ln(Intensity) x ln (power) for the different regions in sample 3.5f. 42
4.2 relation between Intensity and Temperature 42
4.3 O'Donnell 44

List of Figures

1.1 Electronic Bands . . . 18
1.2 States in a Solid . . . 19
1.3 Brillouin Zone . . . 19
1.4 Crystalline Structure . . . 21
1.5 TMDs electronic band. . . . 22
1.6 Exciton features . . . 24
1.7 Semiconductor absorption spectrum . . . 24
1.8 PL and Raman processes . . . 25

2.1 Absorption Coefficient . . . 27
2.2 Exciton binding energy . . . 28
2.3 h-BN . . . 29
2.4 Band Alignment . . . 30
2.5 Heterojunction Lattice . . . 31
2.6 Charge and Energy transfers . . . 32
2.7 Exciton Interlayer . . . 33

3.1 Adhesive tape and Raman . . . 34
3.2 Desirable heterostructure . . . 35
3.3 Transfer System . . . 36
3.4 Optical measurement systems . . . 37
3.5 Samples . . . 37
3.6 Measurements in WITet . . . 38

4.1 Power dependence . . . 40
4.2 Peaks n Excitation Power dependence . . . 41
4.3 Bound excitons . . . 43
4.4 Temperature dependence . . . 45
4.5 Maximum and integrated intensity of PL Spectros . . . 46
4.6 Enhancement of FRET factor . . . 47
4.7 AFM image . . . 49

5.1 Exchange process 51

2 MoS_2 - Fit for the PL spectrums of individual layers for several temperatures 58
3 WS_2 - Fit for the PL spectrums of individual layers for several temperatures 59
4 Fit for the PL spectrums of heterostructures for several temperatures . . 60

List of Abbreviations

ABNT	Associação Brasileira de Normas Técnicas
CB	Banda de Condução (*conduction band*)
CCD	Dispositivo de carga acoplado (*Charge Coupled Device*)
h-BN	Nitreto de Boro hexagonal (*Hexagonal Boron Nitride*)
LCPnano	Laboratório de Caracterização e Processamento de Nanomateriais (*Nanomaterials Characterization and Processing Laboratory*)
MoS_2	Dissulfeto de molibdênio (*molybdenum disulfide*)
SOC	Acoplamento Spin-Órbita (*Spin-Orbit Coupling*)
TMDs	Dicalcogenetos de metais de transição (*Transition metal dichalcogenides*)
UFMG	Universidade Federal de Minas Gerais (*Federal University of Minas Gerais*)
VB	Banda de Valência (*valence band*)
WS_2	Dissulfeto de tungstênio (*Tungsten disulfide*)

List of Symbols

K,Γ	Pontos de alta simetria da zona de Brillouin (*High symmetry Brillouin zone points*)
E_G	Energia do gap
η	Eficiencia Quântica (*Quantum Yield*)

Contents

1 Introduction **17**

1.1 Fundamental concepts . . . 17

1.1.1 Electronic states, band gaps . . . 17

1.1.2 Fermi Level, VB, and CB . . . 18

1.1.3 Brillouin zone and high symmetry points . . . 19

1.2 Motivation . . . 20

1.3 Overview . . . 20

1.3.1 Band structures . . . 21

1.3.2 Excitons . . . 22

1.3.3 Photoluminescence . . . 23

1.3.4 Raman . . . 25

2 TMDs and their architectures **26**

2.1 MoS_2, WS_2 and h-BN . . . 26

2.1.1 MoS_2 and WS_2 . . . 26

2.1.2 h-BN . . . 28

2.2 Heterostructures . . . 29

2.2.1 MoS_2, WS_2 and h-BN heterostructures . . . 30

3 Experimental methods **34**

3.1 Sample fabrication and characterization . . . 34

3.2 Experimental Procedures . . . 36

3.2.1 Experimental Setup . . . 36

3.2.2 Measurement methods . . . 37

4 Data Analysis and Results **39**

4.1 Power dependence . . . 39

4.2 Temperature dependence . . . 40

4.3 Analysis of heterostructure regions . . . 43

5 Conclusion **50**

References 52

Appendixes

Supplementary data 58

Chapter 1

Introduction

The present work will be divided into five chapters. In chapter one, the reader can find a brief introduction to the topic and the basic concepts needed to understand this document. Here we will explain the interest in our work as well as its main idea. The second chapter will present a review of the main features of the Transition Metal Dichalcogenides (TMDs) we used, as well as of the other component of our samples, the hexagonal-boron nitride (h-BN), showing the state of the art of our topic through a summary of the more relevant works in literature. In chapter three we will show and explain the experimental techniques used for the fabrication and measurements of the samples. Chapter four contains all the spectral results and their analysis and finally, in chapter five we will present the conclusions and perspectives of the entire work.

1.1 Fundamental concepts

Here we will introduce some essential concepts to understand the discussion proposed in this dissertation and which will be used on a recurring basis throughout the text.

1.1.1 Electronic states, band gaps

Electrons in an atom have well-defined energy levels given by their electronic orbitals which are obtained by taking out the Hamiltonian eigenstates in Schrodinger's equation. When we look at a solid, we have an enormous number of atoms with an even greater number of electrons; each one of these atoms has orbitals (energy levels) that combine in an enormous number of states forming a quasi-continuum of electronic states that constitutes an electronic band. [Fig 1.1]. These states are interspersed with forbidden energy bands, in other words, energy values where there is no possible energy state that can be occupied by an electron. These forbidden states altogether form the Band Gaps (Fig 1.1 right). In a solid, the bands are filled with electrons according to their electronic distribution respecting the Pauli exclusion, which says that two fermions cannot occupy the same state, and the spin $\frac{1}{2}$ property of electrons, which allows two electrons to have the same energy as long as they have a different spin value($-\frac{1}{2}$ or $\frac{1}{2}$). The filling of these bands is what will define whether a material is classified as a metal, an insulator, or a semiconductor. We define a metal as

a solid in which the filling of electronic states ends in the middle of an allowed band, so there are states accessible to electrons that are energized just above the last filled state. An insulator is defined when the filling of electronic states ends just below a band gap and the separation to the next allowable energy level is very large, so energized electrons have no accessible states to occupy above the last filled state. A semiconductor will be a solid that has its states filled up until very close to the band-gap, being a little below or a little above a band-gap that is not "too large"[1], thus the energized electrons have occupiable states close to the last state and depending on the energy supplied they can "jump" a band-gap to the next state.

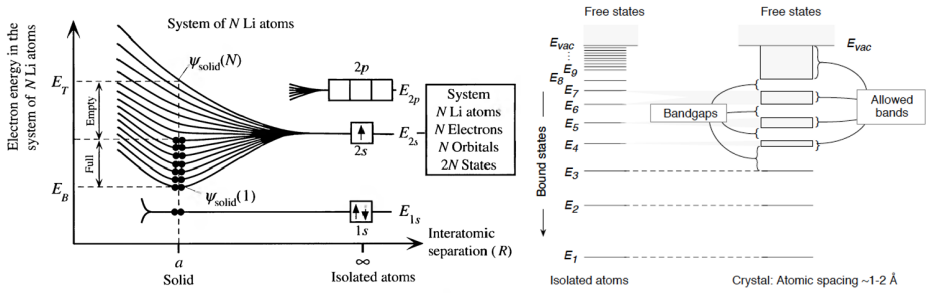

Figure 1.1: *Formation of electronic bands from electronic orbitals. The atomic orbitals (1s; 2s; 2p and so on) from all atoms combine to form a continuum of states (energy values) that the electrons can occupy. taken from [23]*

1.1.2 Fermi Level, VB, and CB

Some definitions are made in order to facilitate the study of solids, such as the Fermi level. The Fermi level is defined as the level, at a temperature of 0 K, where we have the last occupied electronic state. States vary, in energy, with temperature and so another useful definition for the Fermi level is the level where, at a temperature greater than 0 K, we have a state that has a 50% chance of being occupied at any given time. This definition is useful because it is possible to define several quantities and study various electronic behaviors as a function of the Fermi level, for example, one way to define a metal is to say that the solid has the Fermi level placed in the middle of a band.

We define the last filled state as the valence level and the first state subsequent to the valence level as the first conduction level. In semiconductors, the valence level and the conduction level are in different bands and therefore we treat the last filled band as a valence band (VB) and the first unfilled band as a conduction band (CB). We will see that these states are of greater importance because it is in them that the optical and transport effects will take place as described in the section 1.3, with particular importance to the Valence Band Maximum (VBM) and the Conduction Band Minimum (CBM).

[1] The size of a "too large" gap depends on the application, but usually a material with band-gap around 1 eV is considered a semiconductor

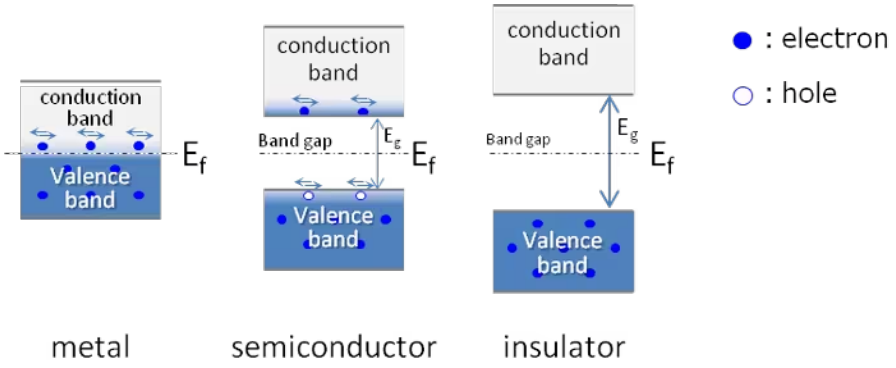

Figure 1.2: *Filling of states in a solid at a temperature greater than 0 K. The distribution of electrons in the solid define what type f material we have. The last state (valence state) occupied by an electron will tell you if we have a metal (The valence state is in the middle of an allowed band), an insulator (the valence state is on the top of a band with a big energy distance until the next available energy state), or a semiconductor (the valence state is on the top of a band with a short energy distance until e next available energy state). Taken from [23]*

1.1.3 Brillouin zone and high symmetry points

When studying crystalline solids, we use the atomic lattice symmetry that can be described in a cell (a group of vectors) that repeats itself periodically building the entire crystalline structure, which we call a Bravais lattice. The Fourier transform of this Bravais lattice gives us another lattice (a set of plane waves) that has the same symmetry operations as the original lattice. We call this lattice a reciprocal lattice and while the first lattice is given in physical space or "position space", the reciprocal lattice is in reciprocal space or "momentum space". This lattice is used to study various properties of the crystal and understand effects such as its x-ray diffraction. The smallest possible vectors that describe the Bravais lattice form what we call a primitive cell. The reciprocal cell to the primitive cell is called the first Brillouin Zone which, as the primitive cell builds the Bravais lattice, builds the reciprocal lattice and therefore the study of electronic states in this zone completely describes the behavior of the crystal. In the first Brillouin Zone, we have some points of

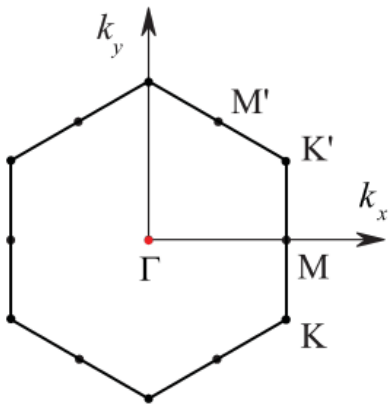

Figure 1.3: *Hexagonal Brillouin Zone and high symmetry points. Figure modified from [60]*

interest due to their high symmetry. These critical points vary according to the Brillouin

Zone format. In a hexagonal Brillouin Zone, the most important points are the points where the edges meet (Point K), the middle of the edges (Point M), and the center (Point Γ) [Fig 1.3]

1.2 Motivation

One of the most important roles of semiconductor physics is to improve the efficiency of existing devices as well as to develop new and better components. In 2004 we had a revolution in the field of semiconductors due to the development of a simple and practical method, with the work of Novoselov et al [38], where they showed how to exfoliate samples of graphite (a known layered material) to the extreme where we obtain a single layer of this material, which was named graphene. Graphene is a material composed of a single layer of carbon atoms, and because of this monatomic thickness, we call it a 2D (two-dimensional) semiconductor. Graphene attracted a lot of attention from the scientific community due to its very interesting characteristics, such as its high electron mobility and mechanical properties, such as flexibility and resistance to tension, and for its characteristic, up until then unique, of being a semiconductor with a linear dispersion of the band at the K points of the Brillouin Zone, and although we call it a semiconductor, it has zero gap. And although this feature is unique, it limits the use of graphene for certain applications, and even though there are ways to expand the graphene gap, a search for semiconductors that have similar dimensions to graphene but that overcome its limitations has arisen. This search opened the door to a whole new science of 2D semiconductors. One of these semiconductor materials that emerged was the TMDs, which contain the central elements of study in this work. These materials have, as we will see below, properties that make them excellent candidates for optoelectronic applications such as amplifiers, transistors, photodetectors, solar cells, Light-Emitting Diodes (LED) and nanoelectromechanical systems, among others.

1.3 Overview

The TMD family is composed of several materials of the MX_2 type, where M is a transition metal and X is a chalcogen (elements of Column 16 in the periodic table), organized in layers in the X-M-X format, that is, with a metal layer sandwiched between two layers of chalcogens (Fig 1.4a). These atomic layers bond together through a strong covalent bond and the bulk is formed by several of these triple layers, which from now on we will treat as a single "monolayer", bonded together by weak Van Der Waals interactions, which allows their mechanical exfoliation. These layers X-M-X can be stacked with different alignments, creating several polytypes, the most interesting being the Trigonal Prismatic (2H), Octahedral (1T) and Rhombohedral (3R)) (Fig 1.4c), a difference that can make the material a semiconductor or a conductor. We will only deal with type 2H semiconductor TMDs here. In this type, as well as graphene, the top view of the monolayer has a hexagonal honeycomb-like shape (Fig 1.4b). Despite not having an isolatable single atomic layer like graphene, TMDs monolayers (3 atoms thick) have dimensions comparable to graphene, which allows us to imagine a whole range of nanotechnologies. They solve the problem of the lack of an energy band gap in graphene. Many TMDs have a non-zero gap with energy

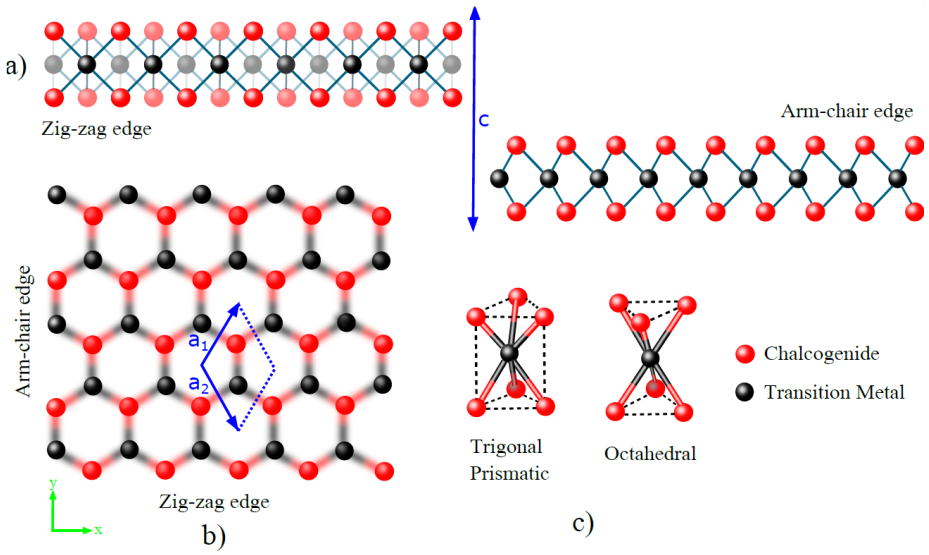

Figure 1.4: *Typical crystalline structure of a TMD with a) the possible crystal edges, arm-chair and zig-zag, from where we can identify the crystalline direction of the TMD. b) A top view of a 2H crystal phase where we see a hexagonal structure, although the crystal is not hexagonal this helps to highlight the primitive cell. c) Two of the possible crystal phases. Together with the rhombohedral phase, these are the most usual phases of TMDs. The semiconductors are usually Trigonal Prismatic. Modified from [31]*

within or close to the visible range. Although many of these materials have been known for several years, in their macroscopic version, a new interest has arisen due to the emergence of unique properties in the monolayer state of these materials. These new properties emerge in some materials due to their dimensionality and interaction between layers that end up generating several effects such as a strong SOC (Spin-orbit coupling), spin valley polarization, high electron mobility, or the transition from indirect gap semiconductors to direct gap semiconductors [Fig 1.5a].

1.3.1 Band structures

Indirect to direct gap transition

One of the main reasons for the interest in these materials is the transition in the electronic gap as we change from bulk (with an indirect gap) to monolayer (with a direct gap)[47]. In general, what we have in these materials is that the shape of the bands is strongly related to the interaction between layers, therefore, when we change the number of layers we are directly modifying the electronic structure of these materials. In Fig 1.5a we can see the transition where the minimum of the conduction band at point K becomes more relevant while the minimum at point Γ loses relevance as we reduce the number of layers. Taking MoS_2 as an example, we can see this clearly in 1.5c. This transition happens because the orbitals that form the states at the point Γ originate from a linear combination of p_z orbitals of sulfur atoms and $d_{z^2 orbitals}$ of molybdenum atoms, where both are delocalized and have an antibonding nature, very present in the interaction between layers. With this, the energy coming from these states is minimized with the decrease of the interaction between layers[34]. On the other hand, the orbitals that generate the states

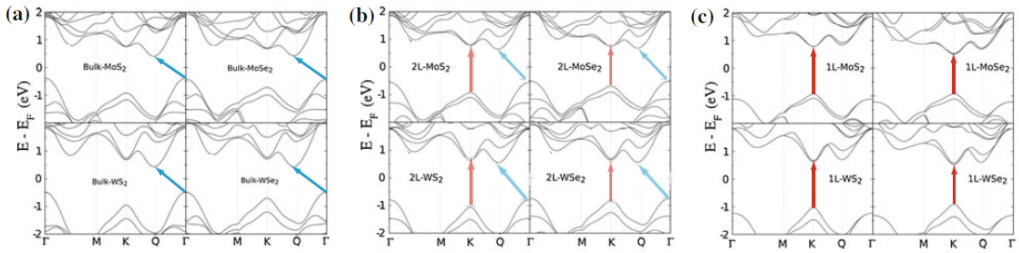

(a) *Indirect to direct gap transition in MoS_2, $MoSe_2$ WS_2 and WSe_2. Q is the direction between the K and Γ high symmetry points.*

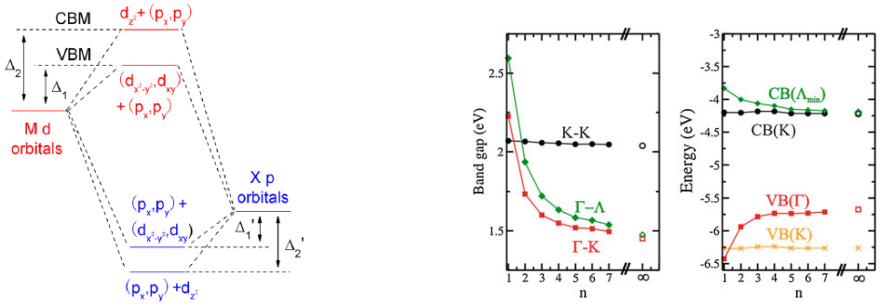

(b) *Schematic of the origin of CBM and VBM in TMDs [21].*

(c) *The energy of the band gap as a function of the number of layers (Left) [41] and the energy of the VBM and CBM in the high symmetry points K, Γ and the direction Λ(Right), which is other notation to the same direction Q used in Fig 1.5a*

Figure 1.5: *TMDs electronic band.*

close to the point K are mainly composed of states located in the xy plane that are not much affected by changes in the $\hat{z}$ direction (perpendicular to the layers)[Fig 1.5c].

SOC and SOS

The valence electrons in the d orbitals of the transition metals in TMDs have high angular momentum that has a strong interaction with the magnetic spin momentum of the electrons. This interaction generates a very strong spin-orbit coupling (SOC) that will be responsible for the strong excitonic emission present in these materials, as we will see later. It is important to note that in these materials, in the 2H phase, when we have an odd number of layers we do not have inversion symmetry, this means that if we take the metallic atom as the center of inversion the chalcogen atoms will be mapped into empty space. This lack of inversion symmetry is responsible, together with the SOC, for lifting the degeneracy in energy, due to spin, existing in both VB and CB at the point **K**. Therefore, we see a spin-orbit splitting (SOS) in energy levels at the K point of the Brillouin zone. SOS plays a fundamental role when studying the excitonic effects of TMDs.

1.3.2 Excitons

Excitons are quasiparticles formed by bonding between an electron excited from the valence band to the conduction band, and a hole (an unfilled electronic state left by the electron) in the valence band. Electrons can be excited in several ways, but the

way that concerns us here and which will be dealt with in the section 1.3.3, is through photoexcitation, where the electron absorbs a photon with energy greater than the bandgap of the material and is promoted to the conduction band and usually decays to the bottom of the conduction band and may form an exciton. We can classify excitons into two types according to their binding energies, which depend a lot on the formation of the bands and also on the dielectric constant of the materials: we have the Frenkel excitons, present in materials with a low dielectric constant, with a small radius (generally the size of the primitive cell) and binding energies from 0.1 eV to 1.0 eV. We also have the Wannier-Mott excitons that are present in materials with a high dielectric constant and large radius, even larger than the lattice spacing, and low binding energies, in the order of 0.01 eV. In TMDs, excitons have strong binding energy, due to their low dimensionality and a strong SOC, which gives them Frenkel exciton characteristics, but we also have reports of delocalized excitons [30] showing characteristics of Wannier-Mott excitons, that are also present in more complex systems, as TMDs heterostructures (section 2.2). Excitons can recombine (the electron decays into the hole) radiatively emitting a photon and not radiatively, through thermal processes involving relaxation mediated by electron-phonon interactions or disassociate through electron transport. Our interest is mainly focused on radiative decay (photoluminescence, section 1.3.3). Excitons can be positively or negatively charged by binding to a hole or an electron, respectively. We call this bound exciton state a trion [Fig 1.6a] and its presence will strongly depend on the number of free charge carriers inside the material, in other words, the relative proportion of trions to excitons is mainly affected by the doping level of the material. We have the possibility of two excitons bonding together creating a state called a biexciton [Fig 1.6b], the formation of this state will depend on the density of excitons in the material. In TMDs excitons play a very important role due to their strong binding energy. Several TMDs exhibit such strong excitonic emission that it is not possible to measure band-to-band recombination where an electron excited in the conduction band decays to the valence band without first having formed an excitonic state.

Some TMDs have two excitonic entities that we call exciton A and exciton B [Fig 1.6a], each one in a different state that arises from the spin-orbit splitting that breaks the degeneracy of energy in VBM and CBM. The exciton A and B are separated by spin selection rules due to the behavior in a high symmetry point that is flipped in spin in relation to the same symmetry point adjacent, this means that the rules are inverse for the K and K' points [Fig 1.6c].

1.3.3 Photoluminescence

There are several ways in which light can interact with matter and as we shed light on a semiconductor, we can observe the optical phenomena of absorption, reflection, and transmission. These effects allow us to collect information concerning the energy band structure and electronic processes in semiconductors [Fig 1.7]. The process of photoluminescence (**??**a) takes place when an electron from the valence band in a semiconductor absorbs a photon, with energy E_{ph} bigger than the energy of the band gap, and it is promoted to the conduction band, leaving a hole in the valence band. After that, the electron, through a process of relaxation (phonon emission, Auger recombination), decays to the bottom of

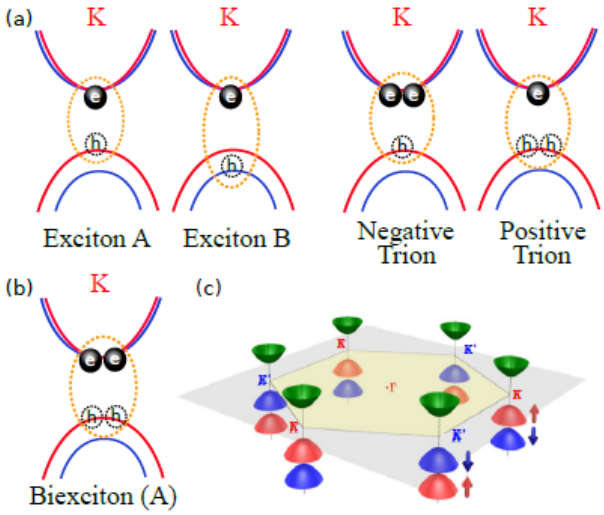

Figure 1.6: *Excitonic features formed in semiconductors. In (a) we have a neutral exciton where an electron in the conducting band is bound to a hole in the valence band and a charged exciton where a carrier is bound to a neutral exciton. In (b) we have two excitons bound together. In (c) we have the spin selection rules that are inverted in adjacent valleys* ***K*** *and* ***K'****. Figure adapted from [55]*

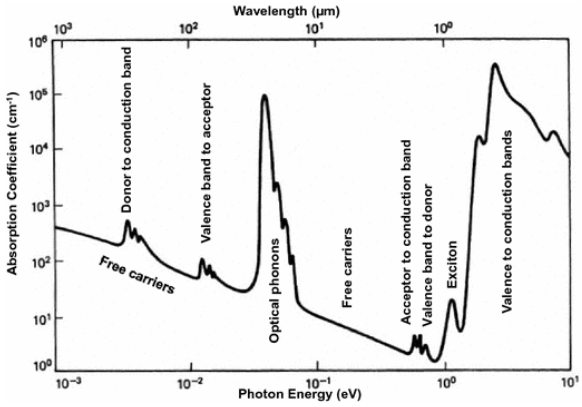

Figure 1.7: *Hypothetical absorption spectrum for a typical semiconductor as a function of photon energy in which we can see the various optical phenomena possible in semiconductors. We will be more interested in the Exciton emissions that are right below the band-to-band absorption edge. Taken from [20]*

the conduction band[2] and then it can lose energy by emitting a photon with the energy of the band gap and decaying again to the valence band recombining with the hole (band to band recombination). There is also the possibility that when the electron gets to the bottom of the conduction band, it interacts with the hole in the valence band and forms an excitonic state (Section 1.3.2) that can recombine radiatively emitting a photon with an energy of the band-gap minus the binding energy of the exciton state, be it a simple state or a more complex one. These emissions constitute PL emissions and give us information such as the size of the band gap, the presence of defects, the binding energy of excitons, and other useful data concerning the band structure of the semiconductor.

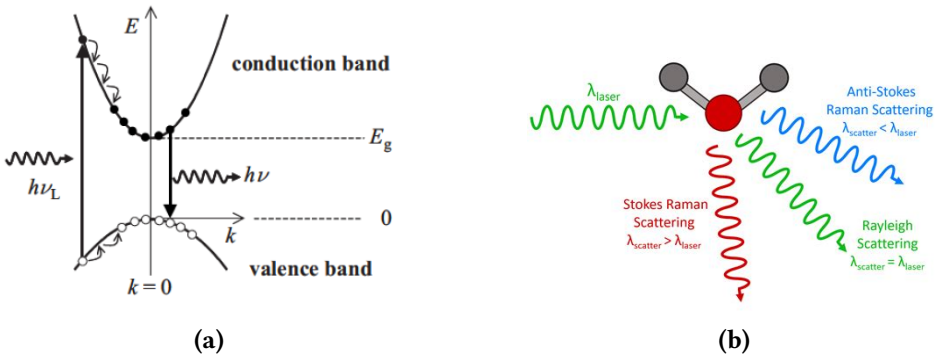

Figure 1.8: *Schematic diagram of the processes occurring during photoluminescence in a direct gap semiconductor(left). Schematic diagram of the Raman Scattering (right).*

1.3.4 Raman

Raman is a technique that uses the interaction between light and matter to study the properties of a material through the vibrations in the lattice. A quasi-particle called a phonon is a collective excitation in a periodic lattice. These quasi-particles can be of two types: acoustic phonons and optical phonons. The phonons can scatter the incident photons in the material. The scattered photons will have higher energy than the incident photon, when a phonon is absorbed in the scattering process, or lower energy when a phonon is generated in the material. The principle of Raman is illuminating a crystal and observing the scattered light to see the photons that gain energy (Anti-Stokes Raman Scattering) or lose energy (Stokes Raman Scattering) in relation to the incident photons (1.8b). This technique is used in the characterization of materials as the phonon dispersion is highly dependent on the structure of the material and sometimes on its configurations, for example, it can be used to determine the number of layers in various TMDs, as we will see in section 3.1.

[2] We can say the same of the hole that relaxes to the top of the valence band with the same momentum as the electron and satisfying the laws of conservation.

Chapter 2

TMDs and their architectures

In this chapter, we will focus on the materials chosen for this work in addition to addressing the properties of heterostructures and the state of the art for this type of architecture.

2.1 MoS_2, WS_2 and h-BN

2.1.1 MoS_2 and WS_2

MoS_2 (molybdenum disulfide) was one of the first TMDs to receive attention, after the graphene boom, and therefore it is the material most explored, with several published papers, both theoretical and experimental. Although there exist various papers on WS_2, its proprieties are not as vastly understood as those of MoS_2. We will now take a look at some of their proprieties.

Mechanical proprieties

There are some experimental studies that measure Young's Module (Table 2.1) of MoS_2 and Ws_2, and various theoretical papers using density-functional theory (DFT) to calculate the mechanical parameters of TMDs. The mechanical properties are relevant to applications in flexible devices and to understand the resistance to strain and impact in these materials.

When we compare Young's Module of these two TMDs (Table 2.1) with some well-known materials such as stainless steel (205 GPa), Kevlar 49 (112 GPa), and graphene (1000 GPa) [28] we see that despite the "monolayer thickness", 2D materials exhibit a large mechanical strength and toughness. This enables the application of 2D materials in various fields. Ultrathin 2D materials with mechanical stability can be used in highly sensitive resonators and flexible electronic devices and, in composites that require high mechanical strength, 2D materials can be used as strengthening additives. Since a few 2D materials show changes in chemical and electrical properties under external mechanical force, various pressure-dependent applications, such as chemical and mechanical sensors and piezoelectric nanogenerators, have been demonstrated based on 2D materials.

Material	Method	Young's (elastic) modulus (GPa)	Reference
MoS_2	DFT	222.75 (a) 219.46 (z) 275.28 (b)	[28]
MoS_2	Experimental	210 ± 100	[1]
WS_2	DFT	244.18 (a) 240.99 (z) 291.62 (b)	[28]
WS_2 nanotubes	Experimental	171	[22]
WS_2 Bulk	Experimental	150	[22]

Table 2.1: *Young's module in the different directions in-plane (a and b) and out-of-plane (z). The mechanical properties are an example of how versatile and promising are these materials.*

Optical properties

Among the many processes that can arise from the light-matter interaction [Fig 1.7], the excitonic processes [Section 1.3.2] are the most relevant for the TMDs [Fig 2.1] due to the strong binding energy of excitons [Table 2.2 and Fig 2.2][1]; emissions from defects bound to excitons also play an important role in low-temperature measurements. Both

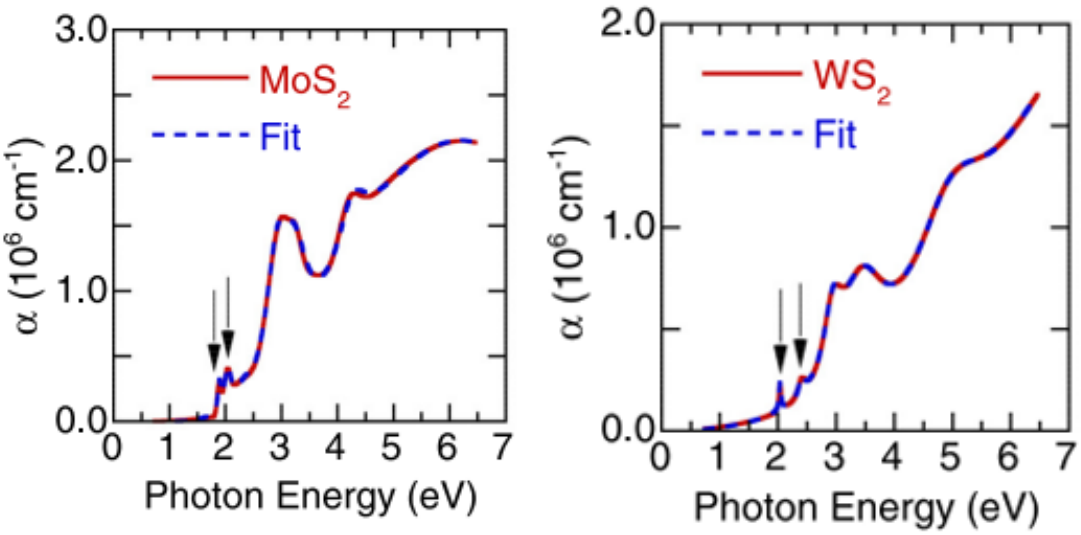

Figure 2.1: *Optical absorption coefficient of monolayer MoS_2 and WS_2 thin films. The arrows denote the exciton peaks. Taken from [29]*

WS_2 and MoS_2 have a large SOS and so two kinds of excitons are observed (Fig 1.6a). In addition, high-intensity emission of the charged exciton A is usually seen (which we will

[1] We can see how large these energies are when we compare them with those on notorious semiconductors such as GaAs, with an exciton binding energy of (4.20 ± 0.3)meV [37]

refer simply as trions since charged excitons B are not very prominent). In some cases, when the conditions (such as the doping level and low thermal energy) are favorable, these materials can show a large density of neutral excitons, and therefore we can detect biexciton emissions (Fig 1.6b)[44, 45].

	MoS_2	WS_2
Optical Band gap (eV)	1.90	2.11
Exciton A BE (eV)	0.28	0.32
Trion BE (meV)	18	26
Biexciton BE (meV)	70	65
SOS VBM (meV)	147	435
SOS CBM (meV)	3	27

Table 2.2: *Experimental values of band-gap and binding energies (BE) of bounded states at TMDs and theoretical values for SOS. Modified from [31] and [24]*

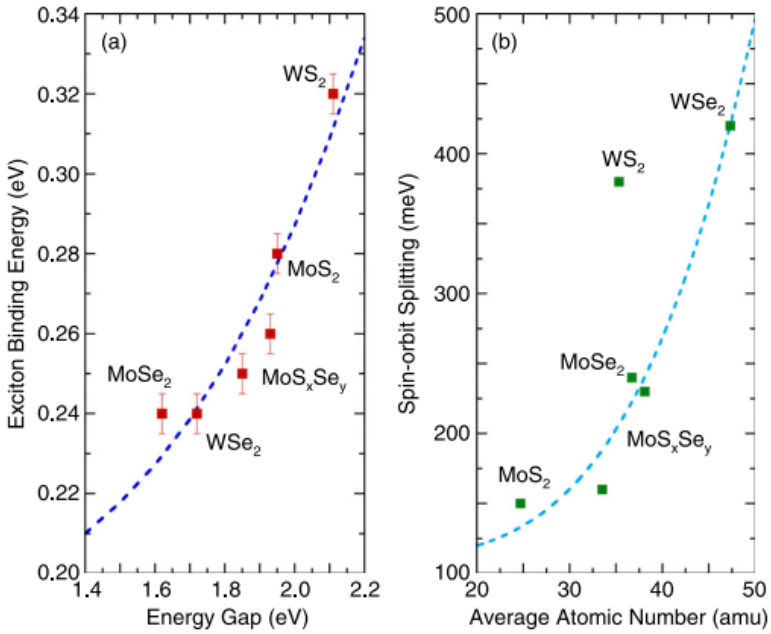

Figure 2.2: *The exciton binding energy as a function of the band-gap energy for different monolayer TMDs (left). The spin-orbit splitting energy as a function of the average atomic number for different TMDs monolayers (right). The dashed lines are fits for the experimental data, following* $E_{BE} = 0.18\ eV + 6.4 * 10^{-3} E_G^4$ *(left) and* $SOS = 115\ meV + 6.0 * 10^{-4} Z_{av}^4$ *(right) where* Z_{av} *is the average atomic number. Taken from [29]*

2.1.2 h-BN

Hexagonal boron-Nitride (h-BN) is another layered material, also analogous to graphene. It consists of a net of rings of three pairs of BN bound by covalent interactions

(Fig 2.3) with the layers held together by Van der Waals interactions. It is an insulator with approximately a 6 eV band-gap, high electrical resistivity (10^{12} – $10^{14}\Omega.cm$), high thermal shock resistance, high thermal conductivity and it is inert to most chemical compounds[9]. The h-BN is commonly used as a substrate or dielectric/separation layer for graphene and other 2D semiconductors, due to a clean interface. Compared to bulk materials, containing rough morphology and dangling bonds on the surface, the h-BN substrate provides reduced local strain and charged impurities. Thus, most 2D materials, such as graphene and MoS_2, exhibit an improved electronic or optoelectronic performance when coupled with h-BN, compared to similar structures built on bulk materials such as silicon dioxide (SiO_2).

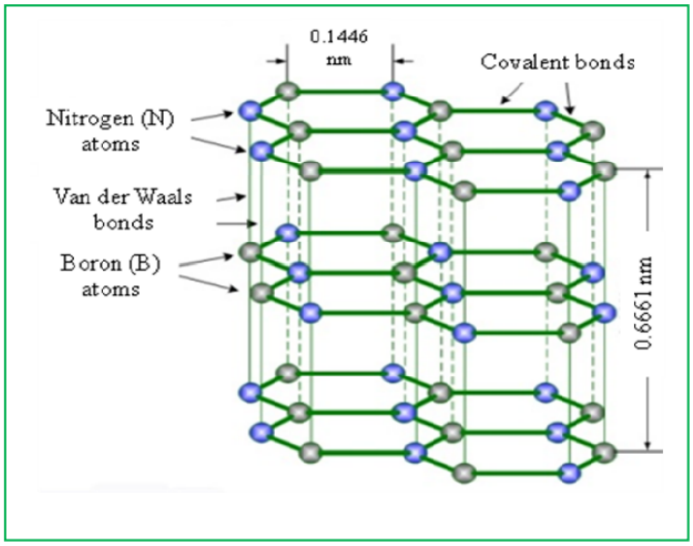

Figure 2.3: *Schematic of hexagonal boron nitride (h-BN) structures We see that the bound inside each layer is strong covalent bonds while the bound of the layer to layer are weak Van der Waals bonds which allows for the exfoliation of this crystal. Taken from [33]*

2.2 Heterostructures

Due to the fact that the interlayer interaction on these materials comes from Van-der-Waals interactions, with no dangling bonds in the plane surface, we do not really need to worry about lattices mismatch when stacking different layers or even with two equal layers but rotated between each other because they bond together with the Van der Waals interaction and have little to none stress caused by the mismatch lattice parameters. We can build a vertical heterostructure as if we were stacking legos [12]. This opens up a huge number of possible combinations of heterojunctions that may produce different and tunable behaviors, applicable to devices [13]. The combination of 2D semiconductors raised attention right since the discovery of other 2D materials after graphene and is still vastly explored, with the most variety of combinations [6, 21, 25, 51] with type I [54] and Type II [16] band alignments. These structures can present new fascinating behaviors, the most attractive being the new-found interlayer excitonic properties as the interlayer excitons that, different from the usual intralayer excitons, possess the hole and the electron spatially delocalized, each one in a different layer of the bilayer structure. This was first reported in stacked monolayers of $MoSe_2$ and WSe_2 where the interlayer excitons were strongly

bound (>100 meV), present long valley depolarization lifetimes (~39 ns), and an exciton lifetime by the nanosecond range [36], 3 times larger than his intralayer counterpart. It was then shown that this heterostructure can possibly form an excitonic Bose-Einstein condensate and present superconductivity, very interesting features that are still in its first stages of study and show potential for the development of valleytronic devices.
It was shown that when you stack TMDs with a little lattice mismatch (as two, or more[3, 43], twisted layers), it emerges a new periodicity in the structure creating what we called a Moiré superlattice [35, 52], and so emerges a new electronic structure that can change the excitonic behavior with new optical responses (as the generation of second harmonic emissions [17]). In this configuration, we can trap interlayer excitons that emit circularly polarized single photons, creating quantum emitters, and in some cases turn dark exciton states into bright excitons [50].

2.2.1 MoS_2, WS_2 and h-BN heterostructures

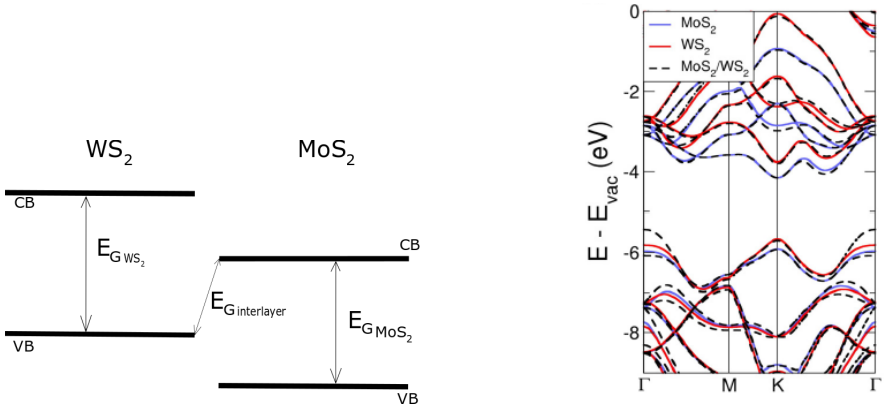

(a) *Type II heterojunction alignment that we can* **(b)** *Overlayed band structures aligned by the Vac-*
use to deduce how the carriers will behave in an uum level. Taken from [6]
excited state.

Figure 2.4: *MoS_2/WS_2 band alignment and electronic bands*

The combination of the materials, presented in the previous sections, in multilayer heterojunctions raises a lot of interest in the scientific community and it has been vastly studied. There have been various attempts to grow vertical and lateral heterojunctions with one or two steps [2, 14, 27, 58, 59]. TMD/h-BN heterojunctions: MoS_2/h-BN [46] and WS_2/h-BN [8], were realized and the TMD/h-BN coupling and the substrate effect were investigated using Raman and PL measurements. The junction from MoS_2 and WS_2 was calculated in [21, 24, 25, 51] and, with a consensus, it was predicted a type II band alignment [Fig 2.4a], with an indirect and a direct interlayer band-gap very close in energy, where the states are localized in two different spacial points: VBM in the K and Γ points of WS_2 and the CBM in the K point of MoS_2 [Fig 2.4b], although some papers say the CBM of the indirect gap is located in the direction Q from the point K to Γ. So we expect to find $K-K$, $K-\Gamma$, and $Q-\Gamma$ transitions beside the usual single monolayer emissions. Experimentally, the junction MoS_2/WS_2 was investigated through PL, Raman and electronic transport [14, 16, 19, 48, 57]. In most of the reports, we observe that both TMDs preserve their excitonic properties, showing themselves to be great candidates

to enhance the performance of existing electronic devices just by adding new layered materials. Furthermore, the structures can present new phenomena as the predicted interlayer exciton interlayers and new Raman modes dependent on the layer alignment [42].

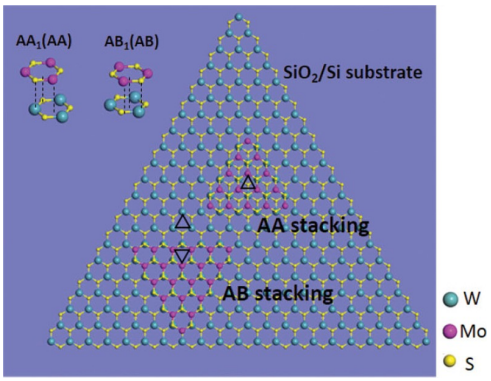

(a) *Stacking modes with 0° (AA Stacking) and 60°(AB Stacking) between layers, which are the two most symmetrical configurations*

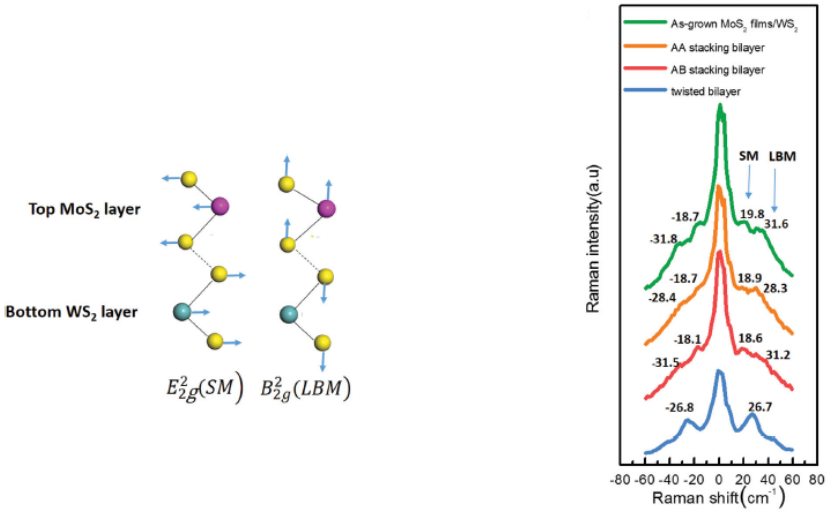

(b) *Representation of active Ramam interlayer* **(c)** *Ramam measurements of SM and LBM (b) for modes that can be used to probe how well coupled aligned (0° and 60°) and mismatched lattices is the heterostructure.*

Figure 2.5: *MoS_2/WS_2 heterojunction superlattice and interlayer Raman modes, taken from [59]*

When there is an alignment of 0° or 60°, we have an **AA** stacking and an **AB** stacking, respectively (Fig 2.5a). These stacking modes show the most efficient coupling with the smaller distance interlayer and with an effective and ultrafast charge transfer[16]. The layer alignment can be evaluated by two Raman modes, a Shear Mode (SM) and a Layer Breathing Mode (LBM) (Fig 2.5b). Besides the Coulombian interlayer interaction with the formation of interlayer excitons, there are two processes that can mediate the interaction between layers. They are the charge transfer and the energy transfer, respectively the Dexter charge transfer [7] and the Förster energy transfer[10] (Fig 2.6a), also known as Fluorescence Resonance Energy Transfer (FRET). In the Dexter transfer process, we need an overlap of the wave functions, given that the charge is exchanged between the acceptor and donor. The transfer rate (K_{ET}) decreases with the layer distance, $K_{ET} \propto e^{\frac{-2r}{L}}$

and due to the non-radiative charge exchange, it is associated with a PL quenching. The FRET process occurs due to a dipole-dipole interaction and it is highly dependent on the oscillator strength from the excitons, the rate of radiative relaxation, the non-radiative relaxation rates and it is more predominant in large distances (more than 0.1 nm) and it is associated with a PL enhancement.

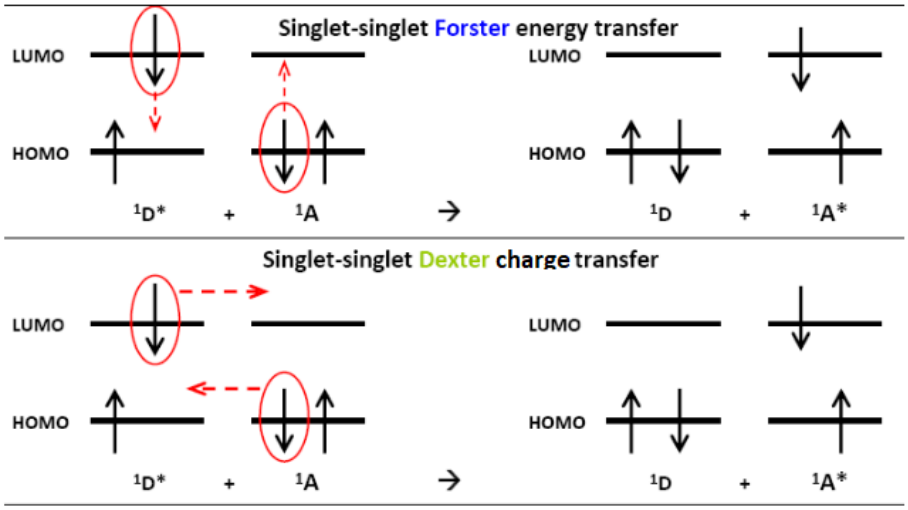

(a) *Schematic of the Föster and Dexter processes, taken from [15]*

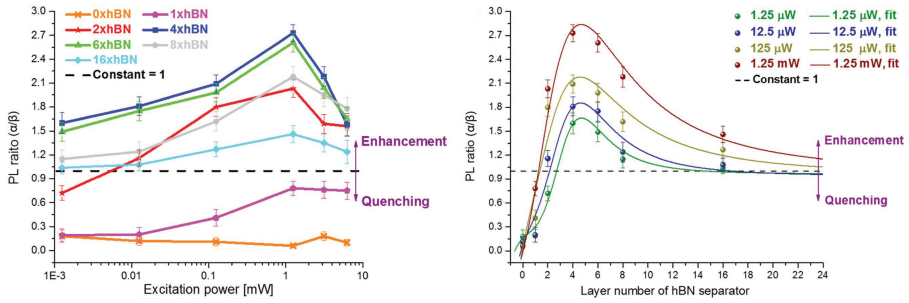

(b) *The PL ratio (PL from junction to single WS_2) as a function of h-BN thickness and excitation power, taken from [57]*

Figure 2.6: *Charge and Energy transfers*

The charge transfer process was investigated in [16, 19, 48] through combined PL mapping and transient absorption measurements, showing a hole transfer time below 50 fs, while the energy transfer mechanism was investigated in [56]. The comparison between the Dexter and Förster processes was investigated in [57] with the use of h-BN as a separator and its noted that with the increase in the h-BN thickness a transition occurs from quenching in the stacking PL to an enhancement in the intensity of the PL (Fig 2.6b right), which are in concordance with the change in the predominance of the energy transfer over the charge transfer with the increase in the layer distance. This transition was also observed with the increase of the excitation power (Fig 2.6b left). This effect is due to the exciton generation rate being directly affected by the increase in the excitation power and so the dipole-dipole interaction overcomes the charge exchange, apart from the dielectric screening that arises from the h-BN layers and obscures the exciton dissociation among the layers.

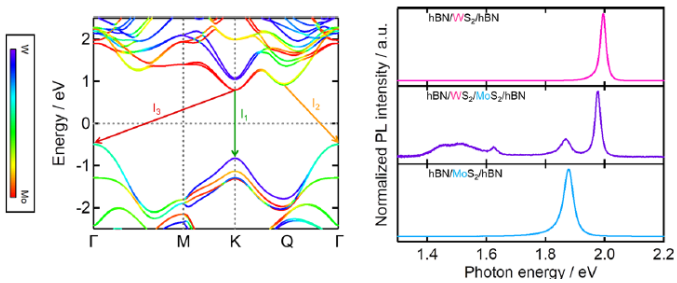

Figure 2.7: *Interlayer band structure (left) and interlayer exciton PL. Taken from [40]*

The interlayer exciton was measured in [40], where it was identified 3 interlayer emissions that come from a direct gap and two indirect gap interlayer transitions (Fig 2.7). The presence of the interlayer emission is strongly dependent of the stacking alignment, as it modifies the interlayer band structure. It was observed that before the formation of the interlayer exciton the charge is transferred with an excess of energy and briefly sustains an intermediate state highly energetic of electron/hole, which we call hot exciton [4]. This extra energy is the reason for the high-efficiency charge transfer and the strong emission of indirect gap interlayer excitons, despite the momentum mismatch between layers. The excess of energy allows a generation of a fast photocurrent considering that the hot exciton possesses a large radius and low binding energy.

Chapter 3

Experimental methods

In this chapter, we will discuss the fabrication and characterization of our samples. We will also show our experimental setup and describe our procedures in the PL measurements.

3.1 Sample fabrication and characterization

The samples were fabricated in the clean room of the Laboratório de Caracterização e Processamento de nanomaterials (LCPnano) located in the Department of Physics of the UFMG. The TMDs were taken from a bulk crystal and placed in adhesive tape [Fig 3.1a]. We then fold the tape gluing it on itself several times, spreading the material throughout the tape. When we have a thin layer of material in the tape we can stick the tape in a square of gel-pak (a Poly(methyl methacrylate), PMMA [11]) to transfer material to the gel. The gel containing the TMDs is then mapped in an optical microscope to search for the monolayers (ML) of the TMD. The first way of identification of the ML is by using optical contrast. The fewer layers it has the more transparent it will appear in the optical microscope. After the selection of some candidate flakes to be a ML, we use, in the same

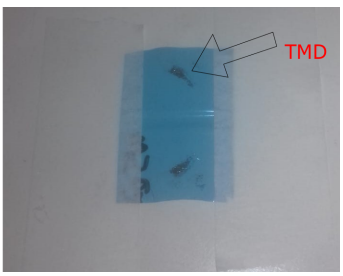

(a) *Tape with a piece of crystal used in the exfoliation process.*

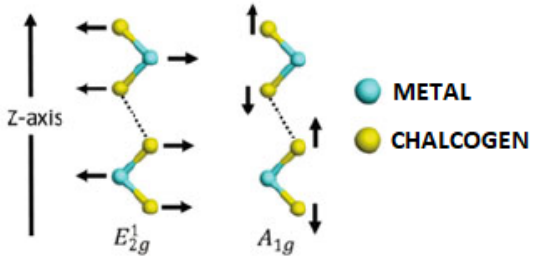

(b) *Multilayer Raman modes A_{1g} and E^1_{2g}. The monolayer retains analogous modes but with the names A'_1 and E' although the bulk nomenclature is commonly used to address its monolayer counterparts. Taken from [31].*

Figure 3.1: *Exfoliation process and active Raman modes used for characterization*

microscope, a Hg lamp with a 546 nm line filter to photo excite the flake. As discussed in section 2.1 the MoS_2 and WS_2 undergo a transition from indirect gap to direct gap as the number of atomic layers is reduced and so, the intensity of luminescence increases considerably from bilayer to monolayer. Using the microscope we can excite the flakes and save the ones that shine brighter under the Hg lamp excitation. This procedure is usually enough to identify the ML and proceed to the next step in the fabrication of the samples. In cases where the fluorescence is not undeceiving enough, we can use Raman Spectroscopy as described in section 1.3.4. Both MoS_2 and WS_2 have two active modes that can be used to determine the number of layers, the modes A_{1g} (an out-of-plane mode) and E^1_{2g} (an in-plane mode) (Figs. 3.1b and 3.6b). As the Raman shift of the modes is dependent on the number of layers, the distance between these two modes is characteristic of the monolayer and increases as we increase the number of layers until it is saturated in the bulk [26]. We use these Raman modes to be sure of the monolayer nature of the flakes but as we will see below, we also use them as a way to determine regions in the heterostructure [Figs. 3.2 and 3.6].

We perform the same procedure of exfoliation with the h-BN, but besides the tape-gel transfer we also perform a direct transfer to a SiO_2/Si substrate, and in this case, we mapped the substrate to find a thick and clean surface h-BN, that can be used as substrate in which we build our heterostructure on top. The gel with h-BN was mapped to find thin flakes with a few layers of h-BN that we use as layers spacer (h-BN2 in fig 3.2). The thickness of the h-BN is only determined by the optical contrast and it's usually a few layers thick (~8-12 layers). With all the flakes selected, we use our transfer system (Fig 3.3)

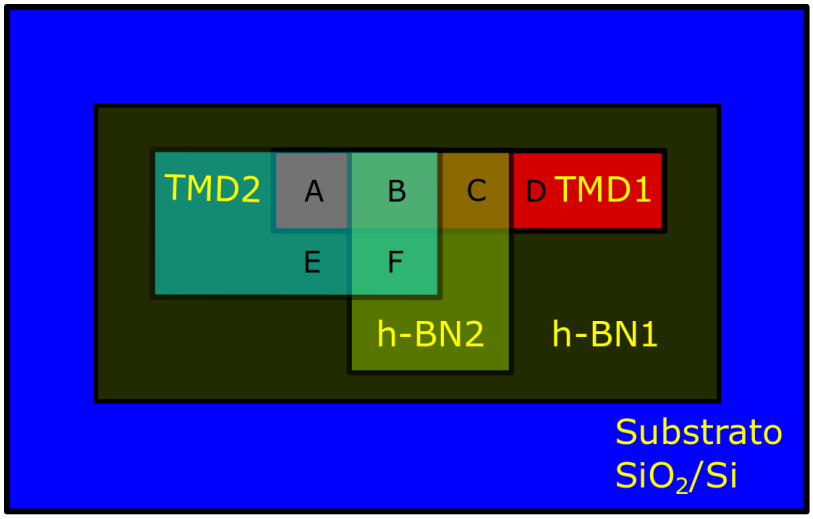

Figure 3.2: *Heterostructure scheme we intend to achieve with the possible regions of contact: A=TMD2/TMD1; B=TMD2/h-BN/TMD1; C=h-BN/TMD1; D=TMD1; E=TMD2; F=TMD2/h-BN. The order of transfer is, from the bottom to the top, h-BN1, TMD1, h-BN2, and TMD2.*

to assemble the heterostructure. We start with the first TMDs (MoS_2 or WS_2) and transfer them atop the h-BN we exfoliated directly in the SiO_2. After that, we transfer the thin h-BN over the first TMD covering only a part of it. In the final transfer, which is the most delicate, we transfer the second TMD trying to place it in a manner to obtain all the regions shown schematically in Fig 3.2. With some variation in this process we create several samples

[Fig. 3.5], sometimes taking of the thin h-BN [Figs. 3.5a and 3.5c], sometimes focusing in aligning the two TDMs by its edges in order to obtain a good coupling [Figs. 3.5f and 3.5g]. There are also samples that are in direct contact with the SiO_2[Figs. 3.5a to 3.5d] i.e., the thick h-BN was removed from the process.

Figure 3.3: *Transfer System used to make the vertical stacking of the samples*

3.2 Experimental Procedures

The measurements were carried out in the characterization laboratory at the LCPnano and in our optical laboratory, both in the Physics Department at the UFMG.

3.2.1 Experimental Setup

The measurements at LCPnano were conducted using a micro-Raman spectrometer (WITec alpha300 RA, fig 3.4b). This equipment is equipped with 633 nm, 532 nm, and 457 nm diode lasers, and we can perform room temperature Raman and PL measurements as simple spectrum or spectra maps. We use Raman spectroscopy to help us identify the different regions as we will see in the next section. The equipment is completely integrated with a spectrometer, a microscope, and a Peltier CCD.

The experimental setup used in our laboratory (Fig 3.4a) allows us to perform optical measurements from high to low temperatures and in a vacuum environment. We can perform simple spectrum or PL maps even at low temperatures. The setup is composed of a CCD, a spectrometer, a camera, an objective (50 or 100 times magnification), a set of mirrors, filters (edge and intensity), and a couple of beam splitters. We can operate with

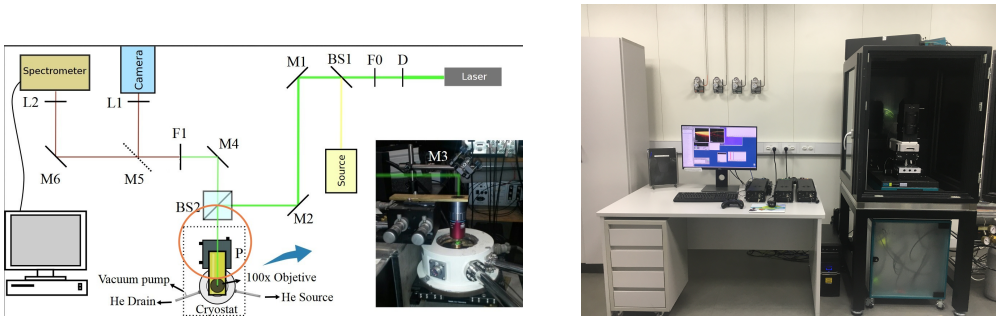

(a) *Experimental Setup* **(b)** *WITec alpha300 RA*

Figure 3.4: *Optical measurement systems*

different lasers for which we use the appropriate set of filters. There is also a cryostat connected to a vacuum pump and an entry to circulate liquid helium or liquid nitrogen in order to refrigerate a cold finger (metal support) where we place the sample. The cryostat is placed in a stage that we can use to center the sample. The objective is connected to a piezo stage and can be dislocated in x,y, and z directions, which helps to centralize the sample. The camera and the spectrometer are both connected to a computer that we use to look at the sample, position it, and control the measurements. To obtain a PL map we use a controller pad to interlink the piezo with the spectrometer and coordinate the movement over the sample with the measurements to execute a PL map.

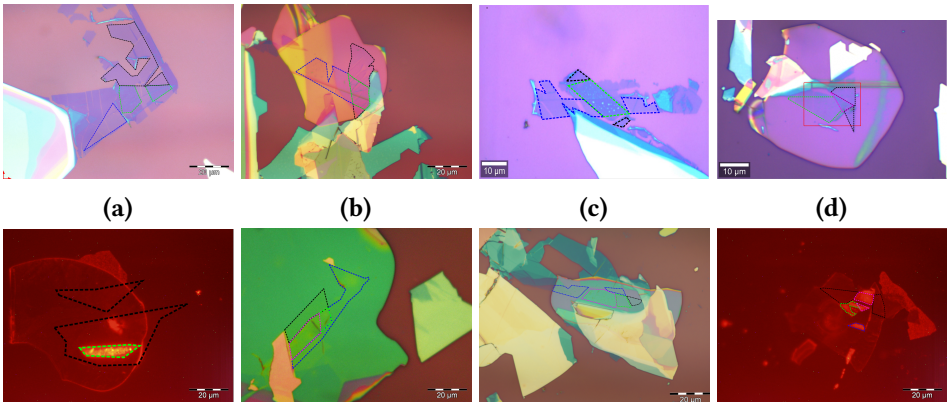

(a) **(b)** **(c)** **(d)**

(e) **(f)** **(g)** **(h)**

Figure 3.5: *Optical and/or fluorescence images (when it was more visually convenient) of some of the fabricated samples in this work, with the different regions highlighted. We use black for MoS_2, blue for WS_2, green for the direct contact of the two TMDs, and purple for the heterostructure with a few layers of h-BN between the two TMDs. With the exception of samples a and c, which are on top of SiO_2, all other samples are on top of an h-BN bulk.*

3.2.2 Measurement methods

The measurements at LCPnano were executed using the 457 nm diode laser at room temperature and atmospheric pressure. We perform Raman measurements to confirm the monolayer nature of our samples and to identify the regions where the monolayers overlap [Fig 3.6].

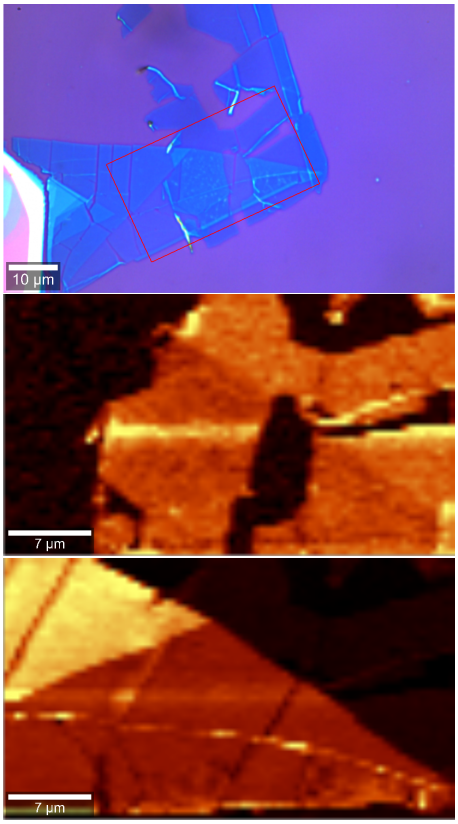

(a) *Raman map of the highlighted area in the optical image on top. Integrated over the MoS_2 Raman peak A_{1g} (middle) and over the WS_2 Raman peak A_{1g} (bottom)*

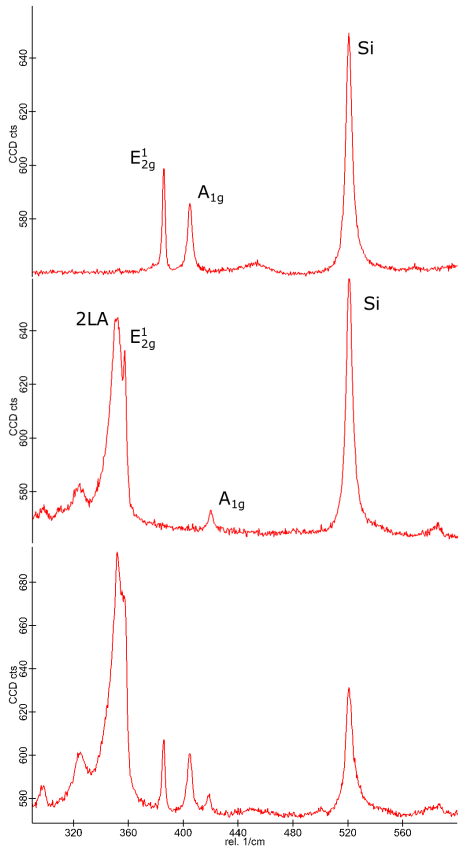

(b) *Raman spectra from different regions: ML MoS_2 (top), ML WS_2 (middle) and from the heterojunction (bottom)*

Figure 3.6: *WITec measurements.*

We also perform room temperature PL using the WITec system. These measurements were used to complement the wider set realized in the optical laboratory. We usually use a laser power in the range of 300 μ W. This is a relatively high power, but it was necessary to make the runtime of the maps workable.
The measurements in the optical laboratory were executed using the 568 nm diode laser with the sample in a vacuum, with the experimental setup shown in Fig. 3.4a. We vary the temperature in the range of ~ 10 K to 300 K, and at low temperature (10 K) we execute power-dependent measurements in the range of (50 $\pm$ 10)μ W to (250 $\pm$ 10)μ W.

Chapter 4

Data Analysis and Results

In this work, we collect the Raman and PL spectra from vertical heterojunctions of WS_2 and MoS_2, using h-BN as a separator from the substrate of SiO_2 and between layers of the TMDs. Here we discuss the results of a typical sample studied during this master's project (Samples 3.5f). In Section 4.1, we examine the nature of the peaks trying to separate the excitons, trions, and excitons bound to defects using the PL dependence with the power excitation. In the section 4.2, we investigate the redshift from the emissions due to the gap dependence with temperature and study the excitonic phenomena and its temperature dependence, and finally, in section 4.3 we compare the emissions from the heterostructure with and without h-BN to the single layers to observe the differences that arise from the interaction between layers.

4.1 Power dependence

Controlling the power excitation we control the density of photons that arrive in the sample and can be absorbed by the valence electrons. Different densities of photons can favor some aspects of the PL spectrum, (such as excitons and biexcitons) while disfavoring some emissions (like excitons bound to defects) The relation between the PL intensity (I) and the incident laser power (P) is given by:

$$I = CP^n, \tag{4.1}$$

where C is a constant and n is the power index. Taking the logarithmic of this equation we have a linear relation:

$$ln(I) = ln(C) + nln(P) \tag{4.2}$$

From this equation, we can analyze the evolution of the PL peaks as a function of the excitation power and, through the valor of n, estimate which excitonic emission the peak corresponds to. For exciton emissions, the n should be close to 1, while for trions it should be between 1 and 2, biexcitons should have an n equal to 2, and for bound excitons, we expected a sublinear behavior. This is because we need one photon to create a pair electron-hole needed to generate an exciton, while for trions is a photon to generate a pair electron-hole and another carrier, i.e. half the effect of a photon, while for biexcitons we

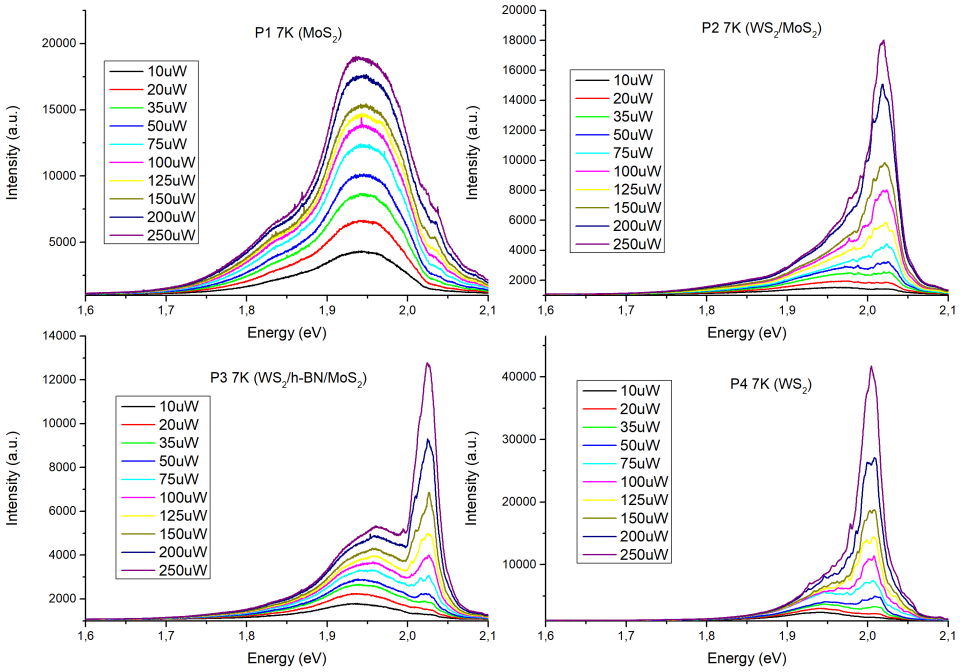

Figure 4.1: *Evolution of the power dependence in the different regions of sample 3.5f using a 568nm laser line.*

need two photos as we need two pair electron-hole for each biexciton.

We can see that each region has a different behavior with the excitation power (Fig. 4.1) and through the spectrum adjustment, we can extract the peaks and identify them in table 4.1. The values for n are as expected in the regions of single TMDs with the peaks were hoping to find, but with a surprising emission of a second trion peak, probably separating the trion peak in the positive and negative charge trion. In the regions of the heterostructure, we observe an increase in the number of peaks and we see two neutron exciton emissions (that are no excitons B) and two trion emissions (that are not a degeneracy of the trion, as in the WS_2 case, because of the energy difference). Although this sample is a true MoS_2/WS_2 heterostructure, the emission from the heterostructure is composed mostly of the WS_2 emission that is far more intense than the MoS_2 emission. Nevertheless, we could be seeing also a MoS_2 exciton emission, which justifies these duplicate features.

4.2 Temperature dependence

The intensity of the emissions from excitons bound to defects, the so-called bound excitons, are directly related to their binding energy, and the temperature. With higher temperatures, we expect that, due to the low binding energy, the bound excitons will dissociate. Therefore, the emissions of these features tend to decrease with the temperature.

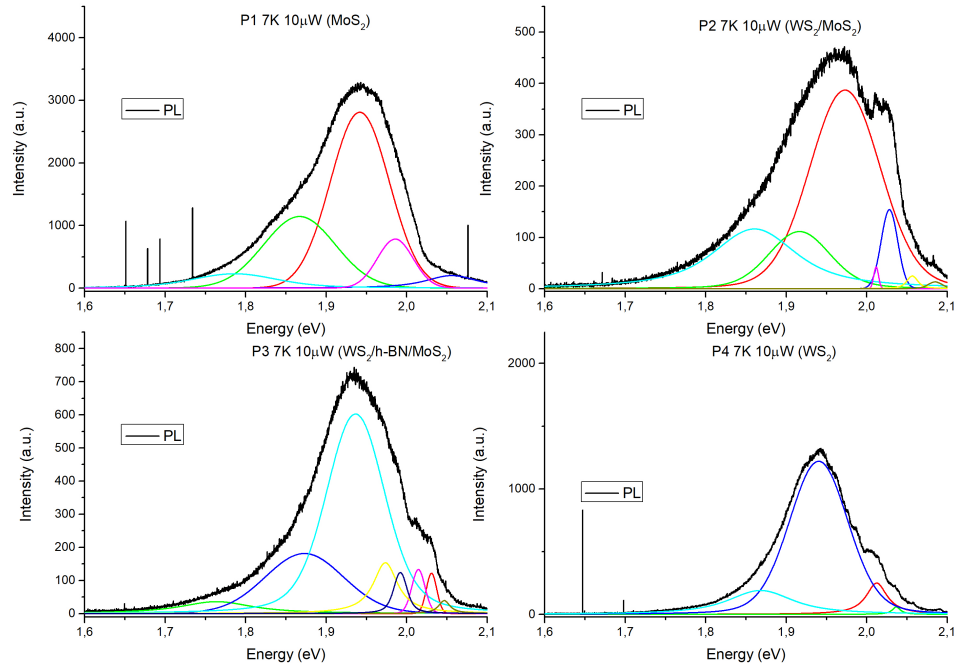

(a) *Peaks in the PL Spectra at 7K with 10μW excitation power.*

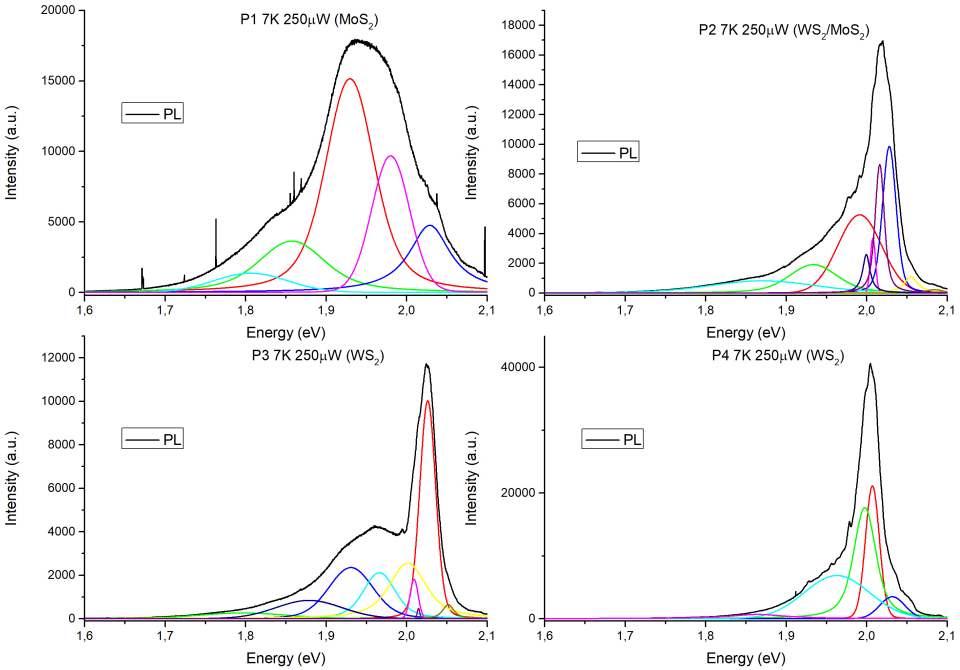

(b) *Peaks in the PL Spectrum at 7K with 250μW excitation power..*

Figure 4.2: *Curve adjusts for the lowest and highest excitation power for the different regions of the sample 3.5f*

	MoS_2	WS_2	$\frac{WS_2}{MoS_2}$	$\frac{WS_2}{\frac{h-BN}{MoS_2}}$
X1	0.72 ± 0.07	1.27 ± 0.08	0.84 ± 0.03	0.81 ± 0.10
X2			0.79 ± 0.08	0.94 ± 0.19
XX			1.96 ± 0.23	
T1	0.99 ± 0.03	1.41 ± 0.09	1.30 ± 0.05	1.36 ± 0.20
T2		1.40 ± 0.11	1.27 ± 0.20	1.05 ± 0.06
L1	0.51 ± 0.01	0.53 ± 0.01	0.74 ± 0.16	0.51 ± 0.07
L2	0.34 ± 0.04	0.34 ± 0.06	0.66 ± 0.06	0.55 ± 0.26
L3	0.56 ± 0.03		0.73 ± 0.05	0.45 ± 0.02
L4				0.46 ± 0.04

Table 4.1: *Slope of the linear relation of ln(Intensity) x ln (power) for the different regions in sample 3.5f.*

This relation can be expressed as:

$$I = Ce^{\frac{-E_{BE}}{k_B T}}, \tag{4.3}$$

where C is a constant, T is the temperature, E_{BE} is the binding energy of the bound exciton and k_B is the Boltzmann constant. If we look at the logarithm of this equation we have a linear relation between the intensity of the emission and the inverse of the temperature:

$$ln(I) = ln(C) - \frac{E_{BE}}{k_B T} \tag{4.4}$$

Using this relation we can confirm the nature of the peaks we believe to be the bound excitons and find their binding energy (Fig 4.3. The parameters we find, shown in Table 2.2, are consistent with bound excitons binding energies ([18]

	MoS_2	WS_2
L1	(20 ± 3)meV	(9 ± 2)meV
L2	(21 ± 3)meV	(16 ± 2)meV
L3	(16 ± 3)meV	(38 ± 4)meV

Table 4.2: *Slope of the linear relation of ln(Intensity) x T^{-1} for the bound excitons in the single regions of TMD's 3.5f .*

We have an increase in the number of emissions in the heterostructure regions and, as we raise the temperature, it became harder to resolve the peaks inside the spectrum, therefore, we did not perform the analysis of equation 4.4 for the heterostructure regions.

The temperature measurements were also used to analyze the evolution of the energy of the emissions as the temperature changes. We know that the band gap of semiconductors changes with the temperature, and despite being hard to make a theoretical model, we have several empirical relations to study the behavior of excitonic emissions in transition

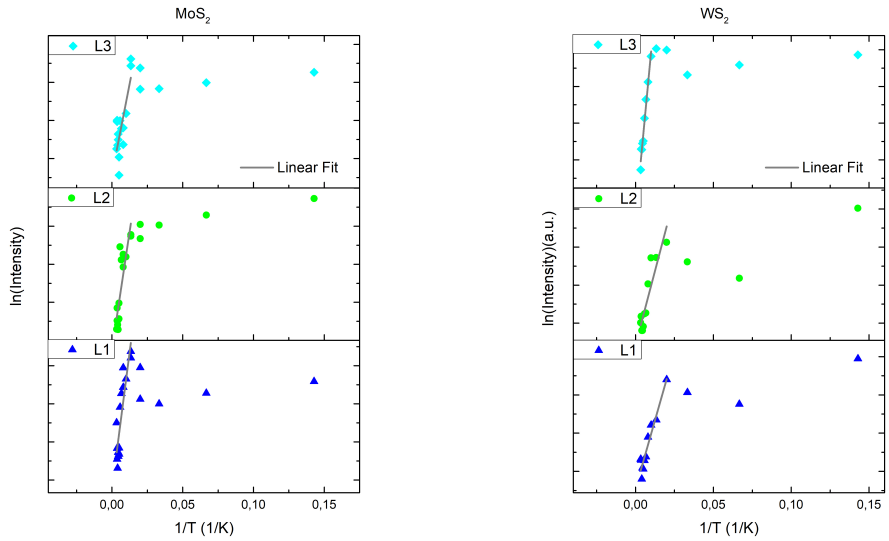

(a) *Bound excitons in MoS_2*

(b) *Bound excitons in WS_2*

Figure 4.3: *Logarithm of the intensity of bound excitons as a function of the inverse of the temperature, with a linear fit in the region of high temperatures.*

metal dichalcogenides. We can use the O'Donnell empirical equation[39]:

$$E_g(T) = E_0 - SE_P\left(coth\left(\frac{E_P}{2k_BT}\right) - 1\right). \tag{4.5}$$

This is an adaptation of the, also empirical, Varnish [53] equation that relates the energy of the band-gap of a semiconductor with the temperature, where E_0 is the gap energy at zero kelvin, and the parameters S and E_P are a dimensionless coupling constant and the average phonon energy, respectively. For our samples, we observe a large number of emissions coming from these excitons bound to defects, which creates a broad emission spectrum; therefore we can not unambiguously separate the emissions, since there are several combinations of peaks that fit the PL spectrum. Here we present one possible adjustment (some of them are shown in Figs. 3 and 4 in the appendice), that we believe better represents the physical phenomena that happened in the heterostructure. Table 4.3 presents the fit parameters obtained from the data shown in Figs. 3 and 4. The parameters obtained are consistent to what is expected, with average phonon energies around tens of meVs and coupling constants of the order of unity.

4.3 Analysis of heterostructure regions

The interactions between the two TMDs that compose the heterostructure are expected to occur through charge transfer and energy transfer (section 2.2.1). We expected that the transfer of energy would occur in both directions and the charge transfer would be of electrons transferring from WS_2 to MoS_2 due to the predicted band alignment (Fig. 2.4a). The emission intensity from the WS_2 alone (I_0) and the intensity in the heterostructure (I) are given by $I_0 = N_W^i \eta_{PL,W}^i$ and $I = N_W^h \eta_{PL,W}^h$, where N and η are the exciton population

		E_P (meV)	S	E_0 (eV)
MoS_2				
	X	48	1.45	2.02
	T	25	0.60	1.98
	L1	13	0.59	1.93
	L2	0.0009	0.45	1.84
WS_2				
	X	49	1.60	2.03
	T	51	1.61	2.01
	L1	0.002	0.83	1.98
	L2	0.0007	1.3	1.96
	L3	16	2.48	1.91
WS_2/MoS_2				
	X	23	2.37	2.19
	T	0.0005	0.78	2.03
	L1	0.0009	1.29	2.02
	L2	0.00003	1.72	1.97
	L3	90	0.21	1.88
WS_2/h-BN/MoS_2				
	X	48	1.45	2.03
	T	25	0.60	1.98
	L1	13	0.59	1.93
	L2	0.00086	0.45	1.84

Table 4.3: *O'Donnell adjust parameters for the curves in Fig. 3, for sample 3.5f) .*

and the PL quantum yield (QY), respectively, for the individual monolayer (index i) and the heterostructure (index h). If we consider an increase in the exciton density in the WS2 layer of the heterostructure due to the energy influx coming from the MoS_2 monolayer through the Föster resonance energy transfer (FRET), the population of excitons in the WS_2 layer of the heterostructure is $N_W^h = N_W^i + N_M^i \eta_{ET,M}$, where $\eta_{ET,M}$ is the QY of the FRET from MoS_2 to WS_2. If we look at the ratio I/I_0, and consider the charge transfer, with QY=$\eta_{CT,W}$, the nonradiative emission, with QY=η_{NR} and the FRET from WS_2 to MoS_2, with QY=$\eta_{ET,W}$ we obtain:

$$\frac{I}{I_0} = (1 + \eta_{ET,M})(1 - \eta_{NR} - \eta_{CT,W} - \eta_{ET,W}). \tag{4.6}$$

The quantum yield for Dexter charge transfer can be written as[57]:

$$\eta_{CT,W} \propto e^{\left(\frac{-2R}{\alpha_B}\right)}, \tag{4.7}$$

and the quantum yield for FRET in 2D systems can be written as[57]:

$$\eta_{ET,W} \propto \frac{1}{1+\left(\frac{R}{R_0}\right)^n}, \tag{4.8}$$

where R is the separation between donor and acceptor, α_B is the exciton Bohr radius and R_0 is the Föster distance, which is the distance where we have 50% of efficiency for the FRET. The exponent n depends on the nature of the dipole-dipole interaction but it is expected to be $2 \leq n \leq 6$. Using all these relations, the equation for the intensity ratio is given by:

$$\frac{I}{I_0} = \left(1 + a_1 \frac{1}{1+\left(\frac{R}{R_0}\right)^n}\right)\left(1 - a_2 - a_3 e^{\left(\frac{-2R}{\alpha_B}\right)} - a_4 \frac{1}{1+\left(\frac{R}{R_0}\right)^n}\right). \tag{4.9}$$

The constants a_1 and a_4 are the FRET coefficients and a_2 and a_3 are the nonradiative decay efficiency of excitons and the charge transfer coefficient, respectively. The values of $R_0 \approx 4,9\ nm$ and $\alpha_B \approx 1.53\ nm$ are reported in literature [49, 57].

If we look at the PL emission intensity from the regions of the heterostructures and compare it to the intensity of the emissions from the individual layer of WS_2, we can observe a distinct behavior for each region (Fig 4.4).

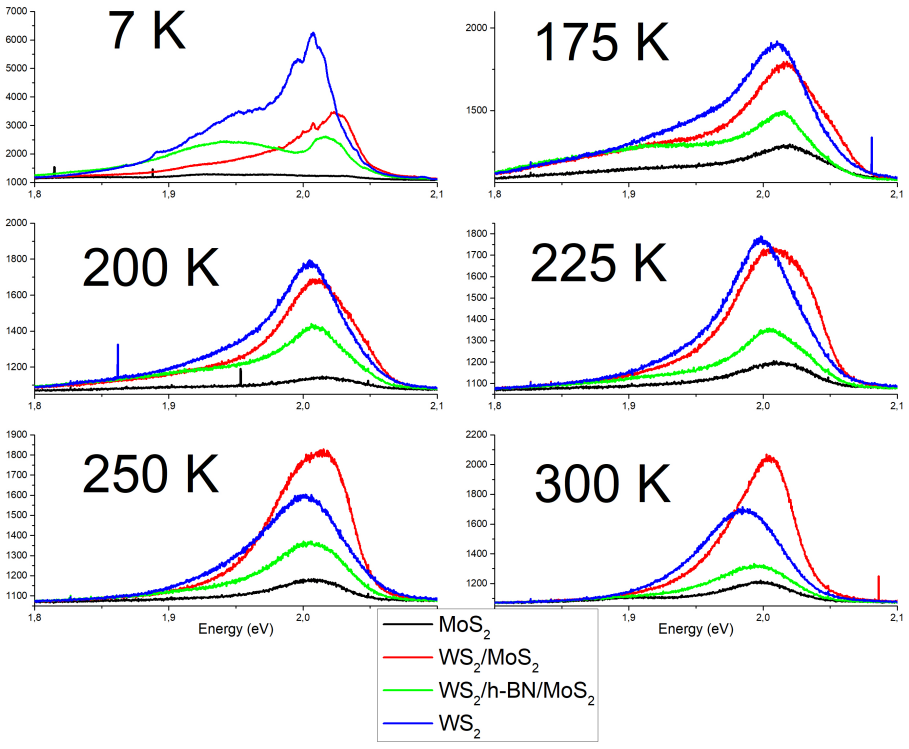

Figure 4.4: *Photoluminescense emissions of the regions in sample 3.5f for several temperatures*

We attribute the difference in luminescence intensity between regions to the exchange processes. Both charge transfer and FRET act on the excitons of the heterostructure to modify the PL emission in relation to that of the individual monolayers. From the region

of direct contact, we observe at low temperatures an emission of lower total intensity than that from WS_2. As the temperature rises, the total intensity of the luminescence from the region of the direct contact heterostructure (red curves in Fig. 4.4) gradually increases relative to the total PL intensity of the sole WS_2 region (blue curves in Fig. 4.4). Above approximately 250 K, the total PL intensity of the direct contact heterostructure is higher than that of the WS_2 monolayer. On the other hand, for the heterostructure with the h-BN spacer (green curves in Fig. 4.4), the total intensity of luminescence is lower than that of the WS_2 monolayer for all temperatures. The luminescence from the MoS_2 monolayer (black curves in Fig 4.5) is of much lower intensity than that from the other regions of the sample, at all temperatures. This relative dependence on temperature of the PL intensities of the different regions of the sample can be more clearly seen in Fig. 4.5, which shows the variation with temperature of the PL peak maximum for each region, relative to that of the WS_2 monolayer (Fig. 4.5 top left) and the integrated luminescence intensity for each region (bottom left), also relative to the integrated PL intensity of the WS_2 monolayer. The right side of Fig. 4.5 shows the evolution with the temperature of the absolute values of PL peak maximum (top right) and integrated intensity (bottom right), for the four regions of the sample. One would expect that the charge transfer process would predominate in

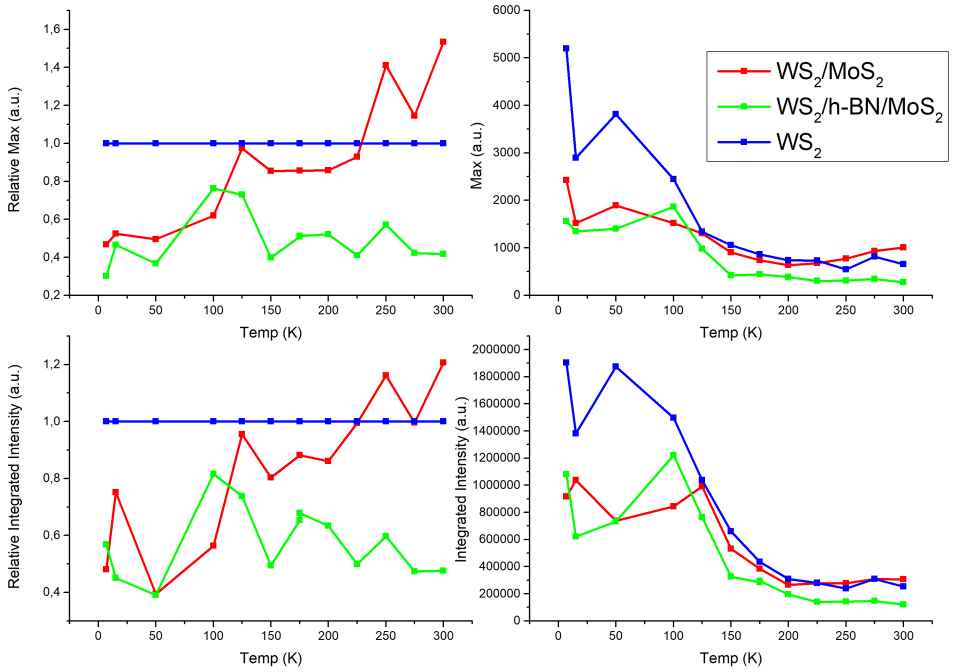

Figure 4.5: *Evolution of the max height of the emissions and the Sum of the spectrum, relative to WS_2 (left) and the absolute value (right)*

the region with direct contact between the TMDs (the direct contact heterostructure) and the FRET process would predominate in the region where the two TMDs are separated by the h-BN layer (heterostructure with the h-BN spacer). However, this behavior is not observed in our sample. The quenching of the luminescence of the heterostructure with

the h-BN spacer, relative to the luminescence of the WS_2 monolayer, indicates that for this heterostructure the charge transfer process plays a more relevant role. In this process, an exciton from the donor (WS_2) dissociates after photogeneration, before recombination, and charge transfer occurs to the acceptor (MoS_2). Due to the predicted band alignment of WS_2/MoS_2, we expect that the electron will be transferred to the MoS_2 layer while the hole remains in the WS_2 side of the heterostructure. The charge transfer process is weakly dependent on temperature, which is in accordance with the weak variation, with temperature, of the PL emission from the heterostructure with an h-BN spacer. The region of the sample where the MoS_2 and WS_2 layers are in direct contact (direct contact heterostructure) exhibits a dependence of the PL intensity on temperature that is what is expected when the FRET process predominates, as it was seen in the work of Medha Dandu et al. [5] and modeled by Lyo [32], assuming an interaction of dipole-dipole between two quantum wells (each of the two bi-dimensional TMDs). This model fits well with the data on the TMD heterostructure of Dandu et al., as shown in Fig. 4.6. The evolution of PL intensity as a function of temperature for the direct contact heterostructure follows this pattern and therefore we propose that for this heterostructure the FRET process predominates over charge transfer.

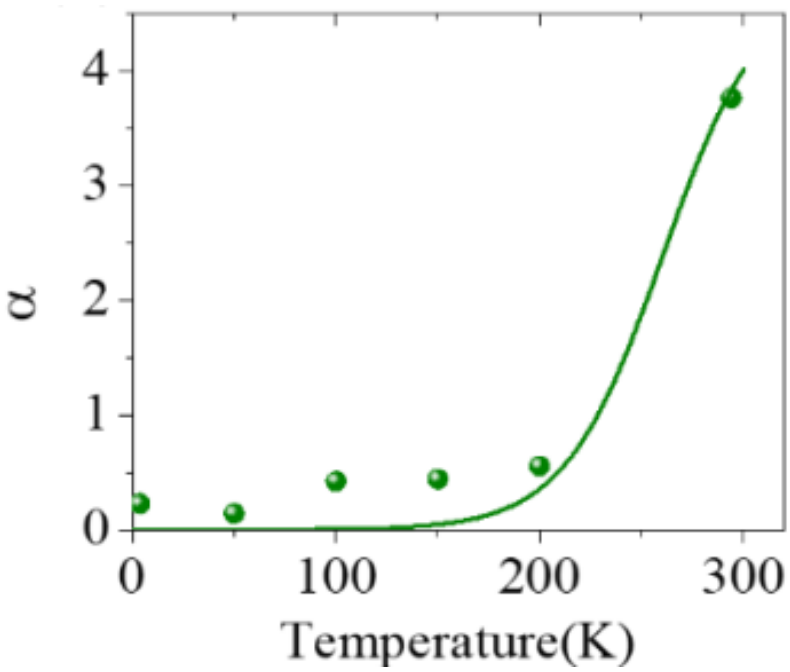

Figure 4.6: *Enhancement factor α from FRET as function of temperature [5]*

The contrasting behavior of the heterostructure with direct contact and the heterostructure with the h-BN spacer, described above, may seem the opposite of what would be expected. But if one looks carefully at the fabrication process of the sample this apparent contradiction can be understood. Charge transfer is highly affected by the coupling between layers, and therefore, impurities, layer alignment, and other factors that can affect the coupling of the layers will also affect the QY of charge transfer. On the other hand, the FRET mechanism is less affected by the coupling of the layers, being more affected by the distance between layers (Equation 4.9). We propose that the region in direct contact in our sample does not have in fact a good coupling between layers and thus the charge transfer

process is not very efficient. Therefore, energy transfer (FRET) dominates the mechanism of exchange for the heterostructure in direct contact.

In the region with the h-BN spacer what we are seeing is the charge transfer process dominating over FRET. That is because the h-BN layer has a smooth surface and is known to reduce defects in the surface of TMDs, leading to an enhancement of their luminescence (see section 2.1.2). Therefore, we expect to have a better coupling between the two TMDs when they are separated by a thin h-BN layer, as is the case of our heterostructure with the h-BN spacer. From an Atomic Force Microscopy measurement (Fig. 4.7a), we estimate the thickness of our h-BN spacer as 6 nm. Thus, we can have the electrons tunneling through the h-BN barrier more efficiently due to the smoothing of the interface. At the same time, the increased distance between the MoS2 and WS2 layers due to the presence of the spacer reduces strongly the effect of energy transfer. The charge transfer mechanism thus predominates and an overall quenching of the luminescence is seen at all temperatures for the heterostructure with the h-BN spacer. From the AFM image, we can also see the abundant presence of contaminants (granular effect in Fig. 4.7b) this can interfere with the coupling of the layers, and as we discuss in the chapter 5 we have to improve the fabrication process to obtain better samples.

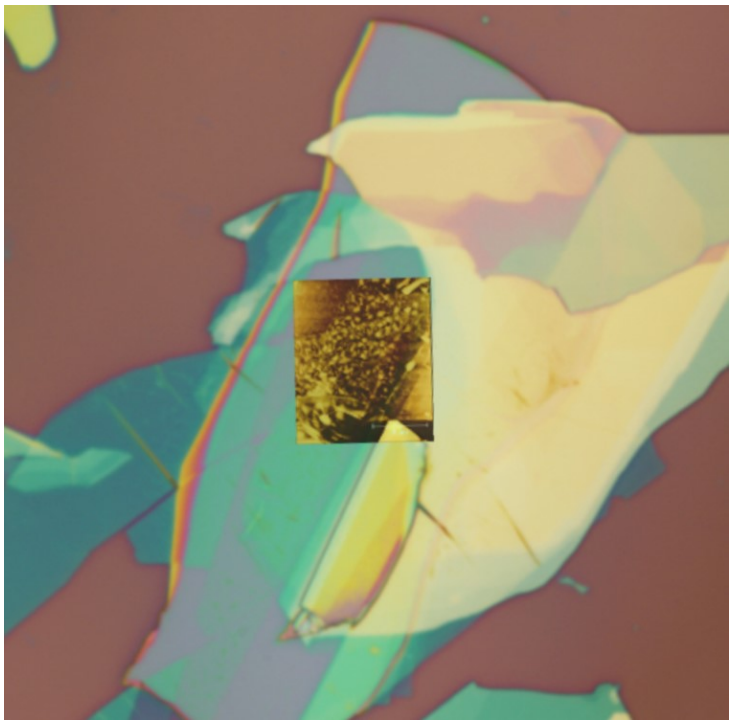

(a) *AFM image over the measured region*

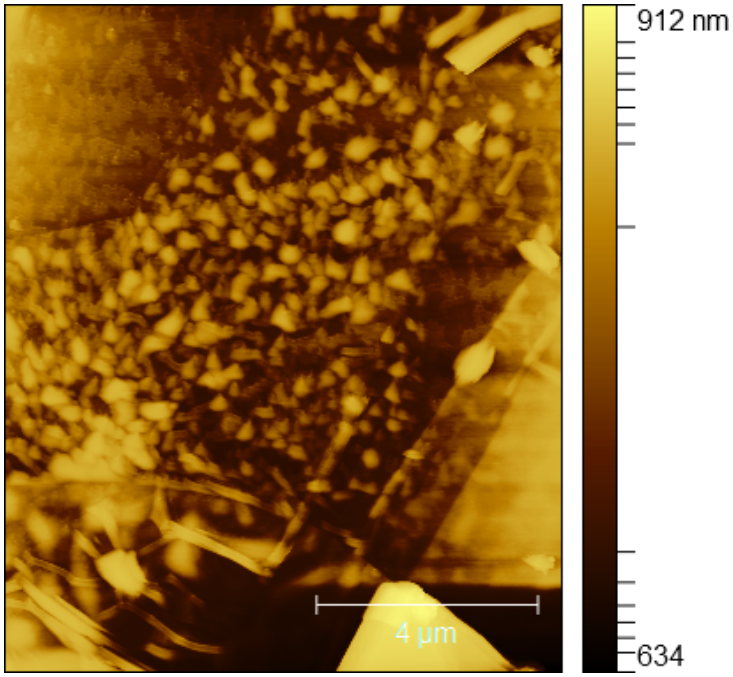

(b) *AFM image*

Figure 4.7: *Atomic force microscopy measurement of sample 3.5f. From the edge profile, we obtain a thickness of* ≈ 1.4 *nm for the* MoS_2, ≈ 1.5 *nm for the* WS_2, *and* ≈ 6 *nm for the h-BN*

Chapter 5

Conclusion

In this work, we investigate the interaction between two monolayers of transition metal dichalcogenides and the effects on the photoluminescence signal. We were particularly interested in the exchange processes in which the two layers can transfer charge and/or energy. We observe different regions with different behaviors where each one of the processes predominates over the other and the factors that contribute to favor each one of the processes. We produced samples through mechanical exfoliation using adhesive tape to exfoliate and a viscous elastic gel to take the samples to an optical microscope and find flakes with low contrast that indicates monolayers. In the interesting flakes, we use fluorescence and Raman spectroscopy to characterize the monolayers. We construct our samples using a vertical transfer process with an alignment to obtain regions of individual TMDs monolayers, overlapped monolayers in direct contact, and with h-BN as a spacer.
We perform photoluminescence measurements varying the temperature from low temperature (7 K) to room temperature (300 K). We also studied the photoluminescence dependence on the excitation power. These measurements give us information about the optical gap as a function of temperature and the behavior of excitonic features from both of the TMDs. The power measurements help us to identify the emissions coming from excitons bound to defects that are a relevant part of the PL spectrum of these materials. From both measurements, we can study the exchange processes when we compare the regions with and without h-BN and note the different behavior from the lower energetic emissions (excitons bound to defects) coming from these two regions and the difference in the PL emission intensity in different temperatures. We noted that the variables from the fabrication of the samples as induced defects and impurities can highly affect the exchange processes, which should be better investigated. The two processes are still not completely distinct and it requires other approaches to help clarify and quantify the interaction between layers of these two TMDs. The interlayer excitons, which we do not explore deeply in this work, can be a great source of information to understand charge transfer, as we expected that the electron that is transferred from one layer to the other will interact with the hole that stayed in the first layer to form these interlayer excitons. Furthermore, the interlayer Raman modes can be used to measure the coupling between the two TMDs. With these pieces of information at hand, we can construct a more complete model based on rate equations to have a better basis on which to construct our hypothesis.
The hardest part of this work was to analyze, identify, and separate the peaks inside the

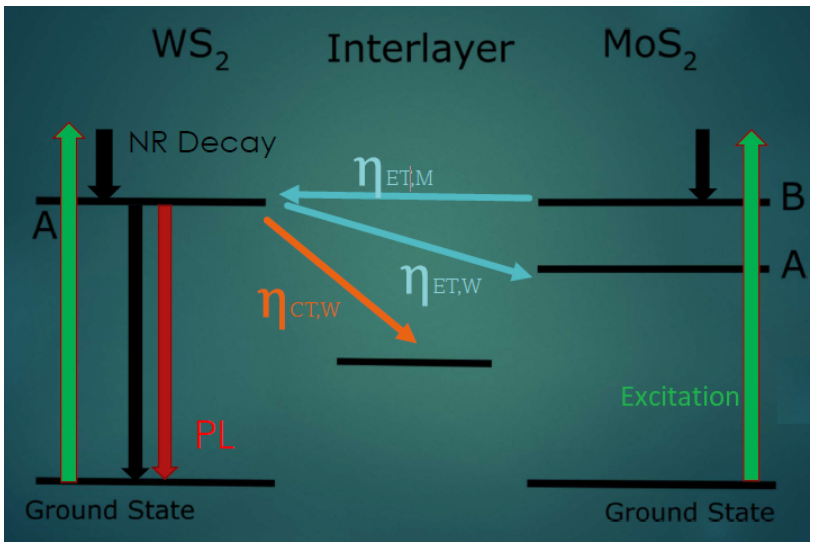

Figure 5.1: *Exchange process with the quantum yield (η) of Energy transfer (**ET**) e charge transfer (**CT**) showed only for one direction, for clarity.*

PL emission. Therefore in the next steps of this project, we intend to perform measurements with time resolution and using the spin selection rules in these materials, exciting resonantly, so we can favor one emission over the other and, therefore, help to identify the emissions, which would help to study the energy transfer mechanism, as the FRET requires an overlap of the wave function, and so, there are certain emissions for which the process is more efficient, as in the case of the exciton B from MoS_2 and the exciton A from WS_2. We can also favor one of the excitonic emissions by applying a back gate to create virtual doping in the heterostructures. The complete understanding of the interlayer interaction of TMDs is of great interest and should be taken ahead. The exchange processes (fig. 5.1) are the foundation for devices based on the emission and also absorption of light. The following steps in this work will be to use Time Resolved measurement to understand the dynamics of the excited states in the heterostructure. We also want to use the spin selection rules combined with resonant polarized excitation to separate and analyze the emissions from the two different materials. We will use the interlayer exciton to understand the charge transfer process and in the future, we want to follow this project with the study of moiré superlattices in these heterojunctions.

References

[1] Simone Bertolazzi, Jacopo Brivio, and Andras Kis. "Stretching and Breaking of Ultrathin MoS2". In: *ACS Nano* 5.12 (2011). PMID: 22087740, pp. 9703–9709. DOI: 10.1021/nn203879f. eprint: https://doi.org/10.1021/nn203879f. URL: https://doi.org/10.1021/nn203879f (cit. on p. 27).

[2] Kevin Bogaert et al. "Diffusion-Mediated Synthesis of MoS2/WS2 Lateral Heterostructures". In: *Nano Letters* 16.8 (2016). PMID: 27438807, pp. 5129–5134. DOI: 10.1021/acs.nanolett.6b02057. eprint: https://doi.org/10.1021/acs.nanolett.6b02057. URL: https://doi.org/10.1021/acs.nanolett.6b02057 (cit. on p. 30).

[3] Frank Ceballos et al. "Highly Efficient and Anomalous Charge Transfer in van der Waals Trilayer Semiconductors". In: *Nano Letters* 17.3 (2017). PMID: 28212486, pp. 1623–1628. DOI: 10.1021/acs.nanolett.6b04815. eprint: https://doi.org/10.1021/acs.nanolett.6b04815. URL: https://doi.org/10.1021/acs.nanolett.6b04815 (cit. on p. 30).

[4] Hailong Chen et al. "Ultrafast formation of interlayer hot excitons in atomically thin MoS2/WS2 heterostructures". In: *NATURE COMMUNICATIONS* 7 (Aug. 2016). ISSN: 2041-1723. DOI: 10.1038/ncomms12512 (cit. on p. 33).

[5] Medha Dandu et al. "Strong Single- and Two-Photon Luminescence Enhancement by Nonradiative Energy Transfer across Layered Heterostructure". In: *ACS Nano* 13.4 (2019). PMID: 30875198, pp. 4795–4803. DOI: 10.1021/acsnano.9b01553. eprint: https://doi.org/10.1021/acsnano.9b01553. URL: https://doi.org/10.1021/acsnano.9b01553 (cit. on p. 47).

[6] Francis H. Davies et al. "Band alignment of transition metal dichalcogenide heterostructures". In: *Phys. Rev. B* 103 (4 Jan. 2021), p. 045417. DOI: 10.1103/PhysRevB.103.045417. URL: https://link.aps.org/doi/10.1103/PhysRevB.103.045417 (cit. on pp. 29, 30).

[7] D. L. Dexter. "A Theory of Sensitized Luminescence in Solids". In: *The Journal of Chemical Physics* 21.5 (Dec. 2004), pp. 836–850. ISSN: 0021-9606. DOI: 10.1063/1.1699044. eprint: https://pubs.aip.org/aip/jcp/article-pdf/21/5/836/11080461/836_1_online.pdf. URL: https://doi.org/10.1063/1.1699044 (cit. on p. 31).

[8] Li Ding et al. "Understanding Interlayer Coupling in TMD-hBN Heterostructure by Raman Spectroscopy". English (US). In: *IEEE Transactions on Electron Devices* 65.10 (Oct. 2018), pp. 4059–4067. ISSN: 0018-9383. DOI: 10.1109/TED.2018.2847230 (cit. on p. 30).

[9] Jens Eichler, Krishna Uibel, and Christoph Lesniak. "Boron Nitride (BN) and Boron Nitride Composites for Applications under Extreme Conditions". In: Advances in Science and Technology 65 (Jan. 2011), pp. 61–69. DOI: 10.4028/www.scientific.net/AST.65.61 (cit. on p. 29).

[10] Th. Förster. "Zwischenmolekulare Energiewanderung und Fluoreszenz". In: *Annalen der Physik* 437.1-2 (1948), pp. 55–75. DOI: https://doi.org/10.1002/andp.19484370105. eprint: https://onlinelibrary.wiley.com/doi/pdf/10.1002/andp.19484370105. URL: https://onlinelibrary.wiley.com/doi/abs/10.1002/andp.19484370105 (cit. on p. 31).

[11] Marta Adriana Forte et al. "Is Poly(methyl methacrylate) (PMMA) a Suitable Substrate for ALD?: A Review". In: *Polymers* 13.8 (2021). ISSN: 2073-4360. DOI: 10.3390/polym13081346. URL: https://www.mdpi.com/2073-4360/13/8/1346 (cit. on p. 34).

[12] A. K. Geim and I. V. Grigorieva. "Van der Waals heterostructures". In: *NATURE* 499.7459 (July 2013), pp. 419–425. ISSN: 0028-0836. DOI: 10.1038/nature12385 (cit. on p. 29).

[13] Cheng Gong et al. "Band alignment of two-dimensional transition metal dichalcogenides: Application in tunnel field effect transistors". In: *Applied Physics Letters* 103.5 (2013), p. 053513. DOI: 10.1063/1.4817409. eprint: https://doi.org/10.1063/1.4817409. URL: https://doi.org/10.1063/1.4817409 (cit. on p. 29).

[14] Yongji Gong et al. "Vertical and in-plane heterostructures from WS2/MoS2 monolayers". In: *NATURE MATERIALS* 13.12 (Dec. 2014), pp. 1135–1142. ISSN: 1476-1122. DOI: 10.1038/NMAT4091 (cit. on p. 30).

[15] Pauline Hibon. "Improving the interface stability of cross-linked films by ink formulation in printed organic light emitting diodes". en. PhD thesis. Darmstadt: Technische Universität, Oct. 2020, iii, 129 Seiten. DOI: https://doi.org/10.25534/tuprints-00014138. URL: http://tuprints.ulb.tu-darmstadt.de/14138/ (cit. on p. 32).

[16] Xiaoping Hong et al. "Ultrafast charge transfer in atomically thin MoS2/WS2 heterostructures". In: *NATURE NANOTECHNOLOGY* 9.9 (Sept. 2014), pp. 682–686. ISSN: 1748-3387. DOI: 10.1038/NNANO.2014.167 (cit. on pp. 29–32).

[17] Wei-Ting Hsu et al. "Second Harmonic Generation from Artificially Stacked Transition Metal Dichalcogenide Twisted Bilayers". In: *ACS NANO* 8.3 (Mar. 2014), pp. 2951–2958. ISSN: 1936-0851. DOI: 10.1021/nn500228r (cit. on p. 30).

[18] Tae Young Jeong et al. "Spectroscopic studies of atomic defects and bandgap renormalization in semiconducting monolayer transition metal dichalcogenides". In: *NATURE COMMUNICATIONS* 10 (Aug. 2019). ISSN: 2041-1723. DOI: 10.1038/s41467-019-11751-3 (cit. on p. 42).

[19] Ziheng Ji et al. "Robust Stacking-Independent Ultrafast Charge Transfer in MoS2/WS2 Bilayers". In: *ACS Nano* 11.12 (2017). PMID: 29116758, pp. 12020–12026. DOI: 10.1021/acsnano.7b04541. eprint: https://doi.org/10.1021/acsnano.7b04541. URL: https://doi.org/10.1021/acsnano.7b04541 (cit. on pp. 30, 32).

[20] Ado Jorio. *Raman Spectroscopy in Graphene Related systems*. 1st ed. WILEY VCH Verlag GmbH and Co. KGaA, 2011 (cit. on p. 24).

[21] Jun Kang et al. "Band offsets and heterostructures of two-dimensional semiconductors". In: *Applied Physics Letters* 102.1 (2013), p. 012111. DOI: 10.1063/1.4774090. eprint: https://doi.org/10.1063/1.4774090. URL: https://doi.org/10.1063/1.4774090 (cit. on pp. 22, 29, 30).

[22] I Kaplan-Ashiri et al. “Mechanical behavior of individual WS2 nanotubes”. In: *JOURNAL OF MATERIALS RESEARCH* 19.2 (Feb. 2004), pp. 454–459. ISSN: 0884-2914. DOI: 10.1557/jmr.2004.19.2.454 (cit. on p. 27).

[23] S. O. Kasap. *Principles of Electronic Materials and Devices*. 3rd ed. University of-Saskatchewan Canada. McGraw-Hill Science, 2005 (cit. on pp. 18, 19).

[24] K. Ko śmider and J. Fernández-Rossier. “Electronic properties of the MoS_2-WS_2 heterojunction”. In: *Phys. Rev. B* 87 (7 Feb. 2013), p. 075451. DOI: 10.1103/PhysRevB.87.075451. URL: https://link.aps.org/doi/10.1103/PhysRevB.87.075451 (cit. on pp. 28, 30).

[25] Hannu-Pekka Komsa and Arkady V. Krasheninnikov. “Electronic structures and optical properties of realistic transition metal dichalcogenide heterostructures from first principles”. In: *Phys. Rev. B* 88 (8 Aug. 2013), p. 085318. DOI: 10.1103/PhysRevB.88.085318. URL: https://link.aps.org/doi/10.1103/PhysRevB.88.085318 (cit. on pp. 29, 30).

[26] Changgu Lee et al. “Anomalous Lattice Vibrations of Single- and Few-Layer MoS2”. In: *ACS Nano* 4.5 (2010). PMID: 20392077, pp. 2695–2700. DOI: 10.1021/nn1003937. eprint: https://doi.org/10.1021/nn1003937. URL: https://doi.org/10.1021/nn1003937 (cit. on p. 35).

[27] Juwon Lee et al. “Thermodynamically Stable Synthesis of Large-Scale and Highly Crystalline Transition Metal Dichalcogenide Monolayers and their Unipolar n–n Heterojunction Devices”. In: *Advanced Materials* 29.33 (2017), p. 1702206. DOI: https://doi.org/10.1002/adma.201702206. eprint: https://onlinelibrary.wiley.com/doi/pdf/10.1002/adma.201702206. URL: https://onlinelibrary.wiley.com/doi/abs/10.1002/adma.201702206 (cit. on p. 30).

[28] Junwen Li, Nikhil V. Medhekar, and Vivek B. Shenoy. “Bonding Charge Density and Ultimate Strength of Monolayer Transition Metal Dichalcogenides”. In: *The Journal of Physical Chemistry C* 117.30 (2013), pp. 15842–15848. DOI: 10.1021/jp403986v. eprint: https://doi.org/10.1021/jp403986v. URL: https://doi.org/10.1021/jp403986v (cit. on pp. 26, 27).

[29] Hsiang-Lin Liu et al. “Optical properties of monolayer transition metal dichalcogenides probed by spectroscopic ellipsometry”. In: *Applied Physics Letters* 105.20 (2014), p. 201905. DOI: 10.1063/1.4901836. eprint: https://doi.org/10.1063/1.4901836. URL: https://doi.org/10.1063/1.4901836 (cit. on pp. 27, 28).

[30] Xiaoze Liu et al. “Strong light-matter coupling in two-dimensional atomic crystals”. In: *NATURE PHOTONICS* 9.1 (Jan. 2015), pp. 30–34. ISSN: 1749-4885. DOI: 10.1038/NPHOTON.2014.304 (cit. on p. 23).

[31] R. R. R. López. “Optical properties of transition metal dichalcogenides on GaAs”. MA thesis. Belo Horizonte, Brasil: Universidade Federal de Minas Gerais, Oct. 2018 (cit. on pp. 21, 28, 34).

[32] S. K. Lyo. “Energy transfer of excitons between quantum wells separated by a wide barrier”. In: *Phys. Rev. B* 62 (20 Nov. 2000), pp. 13641–13656. DOI: 10.1103/PhysRevB.62.13641. URL: https://link.aps.org/doi/10.1103/PhysRevB.62.13641 (cit. on p. 47).

[33] S. Majety et al. “Semiconducting hexagonal boron nitride for deep ultraviolet photonics”. In: *Proceedings of SPIE - The International Society for Optical Engineering* 8268 (Jan. 2012), pp. 70–. DOI: 10.1117/12.914084 (cit. on p. 29).

[34] L. F. Mattheiss. "Band Structures of Transition-Metal-Dichalcogenide Layer Compounds". In: *Phys. Rev. B* 8 (8 Oct. 1973), pp. 3719–3740. DOI: 10.1103/PhysRevB.8.3719. URL: https://link.aps.org/doi/10.1103/PhysRevB.8.3719 (cit. on p. 21).

[35] Leo J. McGilly et al. "Visualization of moire superlattices". In: *NATURE NANOTECHNOLOGY* 15.7 (July 2020), pp. 580+. ISSN: 1748-3387. DOI: 10.1038/s41565-020-0708-3 (cit. on p. 30).

[36] Bastian Miller et al. "Long-Lived Direct and Indirect Interlayer Excitons in van der Waals Heterostructures". In: *Nano Letters* 17.9 (2017). PMID: 28742367, pp. 5229–5237. DOI: 10.1021/acs.nanolett.7b01304. eprint: https://doi.org/10.1021/acs.nanolett.7b01304. URL: https://doi.org/10.1021/acs.nanolett.7b01304 (cit. on p. 30).

[37] S. B. Nam et al. "Free-exciton energy spectrum in GaAs". In: *Phys. Rev. B* 13 (2 Jan. 1976), pp. 761–767. DOI: 10.1103/PhysRevB.13.761. URL: https://link.aps.org/doi/10.1103/PhysRevB.13.761 (cit. on p. 27).

[38] K. S. Novoselov et al. "Electric Field Effect in Atomically Thin Carbon Films". In: *Science* 306.5696 (2004), pp. 666–669. DOI: 10.1126/science.1102896. URL: https://www.science.org/doi/abs/10.1126/science.1102896 (cit. on p. 20).

[39] K. P. O'Donnell and X. Chen. "Temperature dependence of semiconductor band gaps". In: *Applied Physics Letters* 58.25 (1991), pp. 2924–2926. DOI: 10.1063/1.104723. eprint: https://doi.org/10.1063/1.104723. URL: https://doi.org/10.1063/1.104723 (cit. on p. 43).

[40] Mitsuhiro Okada et al. "Direct and Indirect Interlayer Excitons in a van der Waals Heterostructure of hBN/WS2/MoS2/hBN". In: *ACS Nano* 12.3 (2018). PMID: 29481065, pp. 2498–2505. DOI: 10.1021/acsnano.7b08253. eprint: https://doi.org/10.1021/acsnano.7b08253. URL: https://doi.org/10.1021/acsnano.7b08253 (cit. on p. 33).

[41] J. E. Padilha et al. "Nature and evolution of the band-edge states in MoS_2: From monolayer to bulk". In: *Phys. Rev. B* 90 (20 Nov. 2014), p. 205420. DOI: 10.1103/PhysRevB.90.205420. URL: https://link.aps.org/doi/10.1103/PhysRevB.90.205420 (cit. on p. 22).

[42] Sangyeon Pak et al. "Strain-Mediated Interlayer Coupling Effects on the Excitonic Behaviors in an Epitaxially Grown MoS2/WS2 van der Waals Heterobilayer". In: *Nano Letters* 17.9 (2017). PMID: 28832158, pp. 5634–5640. DOI: 10.1021/acs.nanolett.7b02513. eprint: https://doi.org/10.1021/acs.nanolett.7b02513. URL: https://doi.org/10.1021/acs.nanolett.7b02513 (cit. on p. 31).

[43] Shudi Pan et al. "Efficient interlayer electron transfer in a MoTe2/WS2/MoS2 trilayer heterostructure". In: *Applied Physics Letters* 118.25 (2021), p. 253106. DOI: 10.1063/5.0047909. eprint: https://doi.org/10.1063/5.0047909. URL: https://doi.org/10.1063/5.0047909 (cit. on p. 30).

[44] Juhi Pandey and Ajay Soni. "Unraveling biexciton and excitonic excited states from defect bound states in monolayer MoS2". In: *Applied Surface Science* 463 (2019), pp. 52–57. ISSN: 0169-4332. DOI: https://doi.org/10.1016/j.apsusc.2018.08.205. URL: https://www.sciencedirect.com/science/article/pii/S0169433218323493 (cit. on p. 28).

[45] I. Paradisanos et al. "Room temperature observation of biexcitons in exfoliated WS2 monolayers". In: *Applied Physics Letters* 110.19 (2017), p. 193102. DOI: 10.1063/1.4983285. eprint: https://doi.org/10.1063/1.4983285. URL: https://doi.org/10.1063/1.4983285 (cit. on p. 28).

[46] Hamin Park et al. “Probing temperature-dependent interlayer coupling in a MoS2/h-BN heterostructure”. In: *NANO RESEARCH* 13.2 (Feb. 2020), pp. 576–582. ISSN: 1998-0124. DOI: 10.1007/s12274-020-2658-3 (cit. on p. 30).

[47] H. S. S. Ramakrishna Matte et al. “MoS2 and WS2 Analogues of Graphene”. In: *Angewandte Chemie International Edition* 49.24 (), pp. 4059–4062. DOI: https://doi.org/10.1002/anie.201000009. URL: https://onlinelibrary.wiley.com/doi/abs/10.1002/anie.201000009 (cit. on p. 21).

[48] Albert F. Rigosi et al. “Probing Interlayer Interactions in Transition Metal Dichalcogenide Heterostructures by Optical Spectroscopy: MoS2/WS2 and MoSe2/WSe2”. In: *Nano Letters* 15.8 (2015). PMID: 26186085, pp. 5033–5038. DOI: 10.1021/acs.nanolett.5b01055. eprint: https://doi.org/10.1021/acs.nanolett.5b01055. URL: https://doi.org/10.1021/acs.nanolett.5b01055 (cit. on pp. 30, 32).

[49] Andreas V. Stier et al. “Exciton diamagnetic shifts and valley Zeeman effects in monolayer WS2 and MoS2 to 65 Tesla”. In: *NATURE COMMUNICATIONS* 7 (Feb. 2016). ISSN: 2041-1723. DOI: 10.1038/ncomms10643 (cit. on p. 45).

[50] Alexander Tartakovskii. “Excitons in 2D heterostructures”. In: *NATURE REVIEWS PHYSICS* 2.1 (Jan. 2020), pp. 8–9. DOI: 10.1038/s42254-019-0136-1 (cit. on p. 30).

[51] Humberto Terrones, Florentino Lopez-Urias, and Mauricio Terrones. “Novel hetero-layered materials with tunable direct band gaps by sandwiching different metal disulfides and diselenides”. In: *SCIENTIFIC REPORTS* 3 (Mar. 2013). ISSN: 2045-2322. DOI: 10.1038/srep01549 (cit. on pp. 29, 30).

[52] Kha Tran et al. “Evidence for moire excitons in van der Waals heterostructures”. In: *NATURE* 567.7746 (Mar. 2019), pp. 71+. ISSN: 0028-0836. DOI: 10.1038/s41586-019-0975-z (cit. on p. 30).

[53] Y.P. Varshni. “Temperature dependence of the energy gap in semiconductors”. In: *Physica* 34.1 (1967), pp. 149–154. ISSN: 0031-8914. DOI: https://doi.org/10.1016/0031-8914(67)90062-6. URL: https://www.sciencedirect.com/science/article/pii/0031891467900626 (cit. on p. 43).

[54] Lingling Wu et al. “Ultrafast Energy Transfer of Both Bright and Dark Excitons in 2D van der Waals Heterostructures Beyond Dipolar Coupling”. In: *ACS Nano* 13.2 (2019). PMID: 30715845, pp. 2341–2348. DOI: 10.1021/acsnano.8b09059. eprint: https://doi.org/10.1021/acsnano.8b09059. URL: https://doi.org/10.1021/acsnano.8b09059 (cit. on p. 29).

[55] Di Xiao et al. “Coupled Spin and Valley Physics in Monolayers of MoS_2 and Other Group-VI Dichalcogenides”. In: *Phys. Rev. Lett.* 108 (19 May 2012), p. 196802. DOI: 10.1103/PhysRevLett.108.196802. URL: https://link.aps.org/doi/10.1103/PhysRevLett.108.196802 (cit. on p. 24).

[56] Wenshuo Xu et al. “Controlling Photoluminescence Enhancement and Energy Transfer in WS2:hBN:WS2 Vertical Stacks by Precise Interlayer Distances”. In: *Small* 16.3 (2020), p. 1905985. DOI: https://doi.org/10.1002/smll.201905985. eprint: https://onlinelibrary.wiley.com/doi/pdf/10.1002/smll.201905985. URL: https://onlinelibrary.wiley.com/doi/abs/10.1002/smll.201905985 (cit. on p. 32).

[57] Wenshuo Xu et al. “Determining the Optimized Interlayer Separation Distance in Vertical Stacked 2D WS2:hBN:MoS2 Heterostructures for Exciton Energy Transfer”. In: *Small* 14.13 (2018), p. 1703727. DOI: https://doi.org/10.1002/smll.201703727 (cit. on pp. 30, 32, 44, 45).

[58] Yunzhou Xue et al. “Scalable Production of a Few-Layer MoS2/WS2 Vertical Heterojunction Array and Its Application for Photodetectors”. In: *ACS Nano* 10.1 (2016). PMID: 26647019, pp. 573–580. DOI: 10.1021/acsnano.5b05596. eprint: https://doi.org/10.1021/acsnano.5b05596. URL: https://doi.org/10.1021/acsnano.5b05596 (cit. on p. 30).

[59] Jing Zhang et al. “Observation of Strong Interlayer Coupling in MoS2/WS2 Heterostructures”. In: *Advanced Materials* 28.10 (2016), pp. 1950–1956. DOI: https://doi.org/10.1002/adma.201504631. URL: https://onlinelibrary.wiley.com/doi/abs/10.1002/adma.201504631 (cit. on pp. 30, 31).

[60] Z. Y. Zhu, Y. C. Cheng, and U. Schwingenschlögl. “Giant spin-orbit-induced spin splitting in two-dimensional transition-metal dichalcogenide semiconductors”. In: *Phys. Rev. B* 84 (15 Oct. 2011), p. 153402. DOI: 10.1103/PhysRevB.84.153402. URL: https://link.aps.org/doi/10.1103/PhysRevB.84.153402 (cit. on p. 19).

Supplementary data

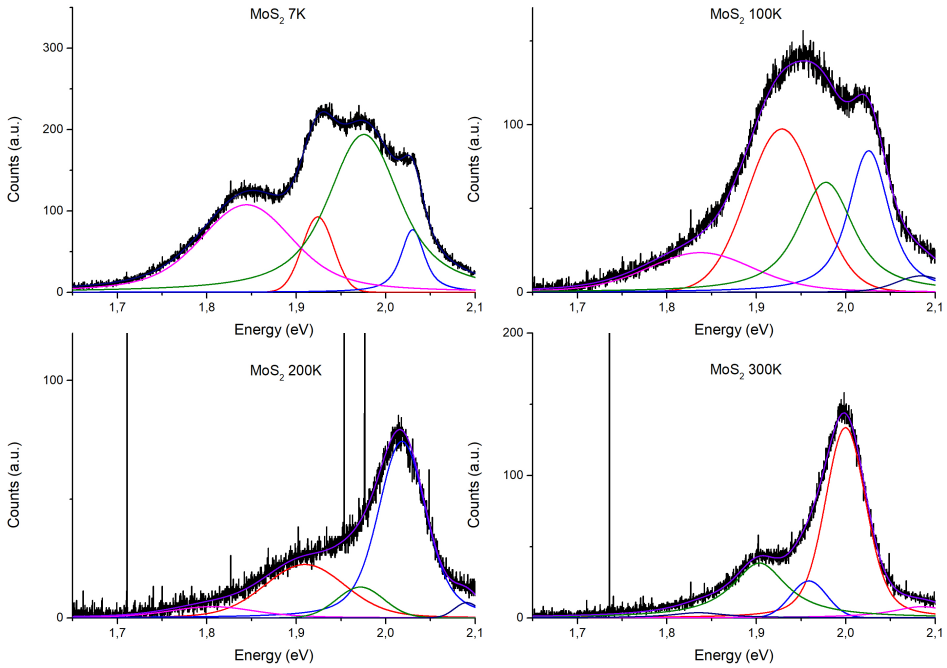

Figure 2: *MoS_2 - Fit for the PL spectrums of individual layers for several temperatures*

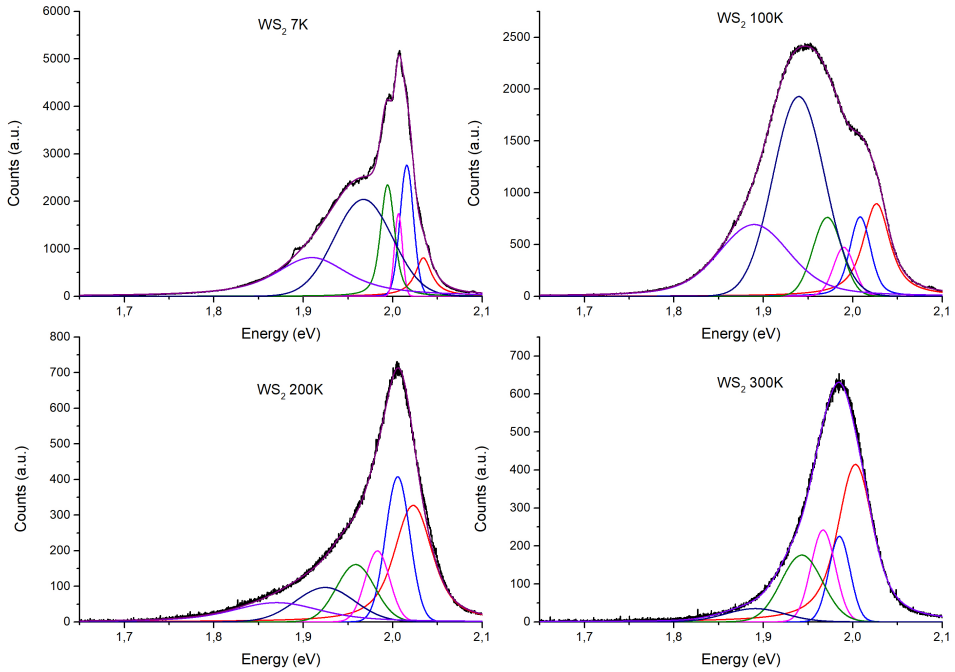

Figure 3: *WS_2 - Fit for the PL spectrums of individual layers for several temperatures*

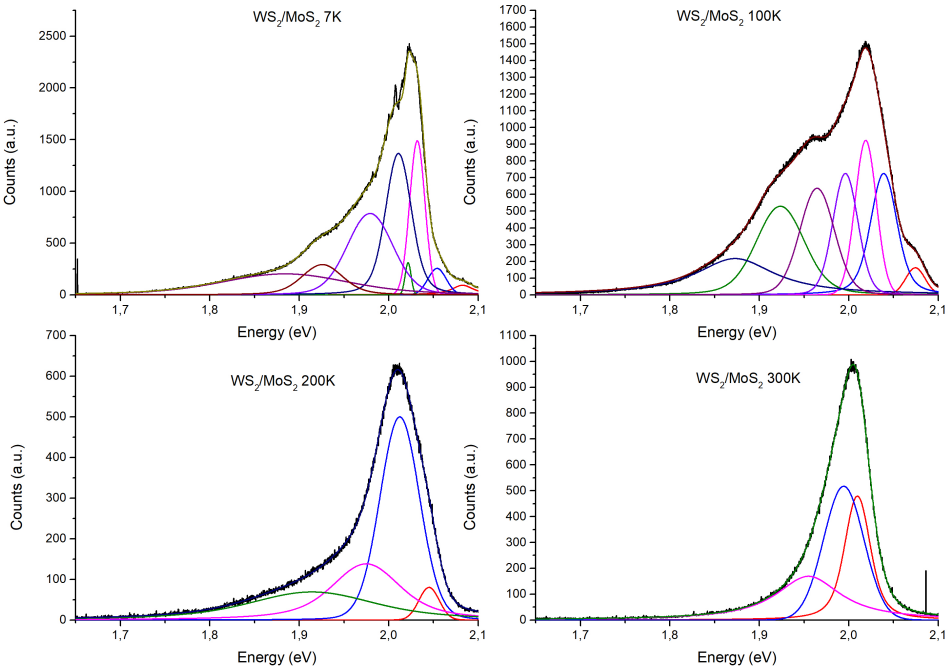

(a) *WS_2/MoS_2*

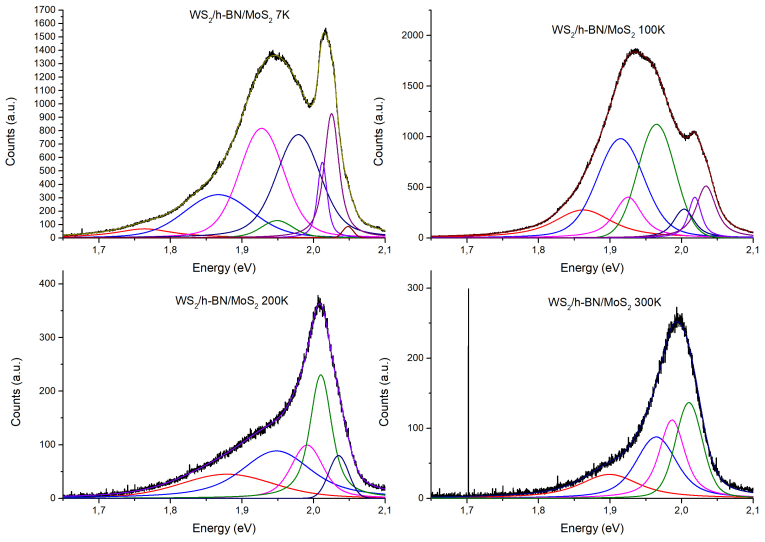

(b) *WS_2/h-BN/MoS_2*

Figure 4: *Fit for the PL spectrums of heterostructures for several temperatures*